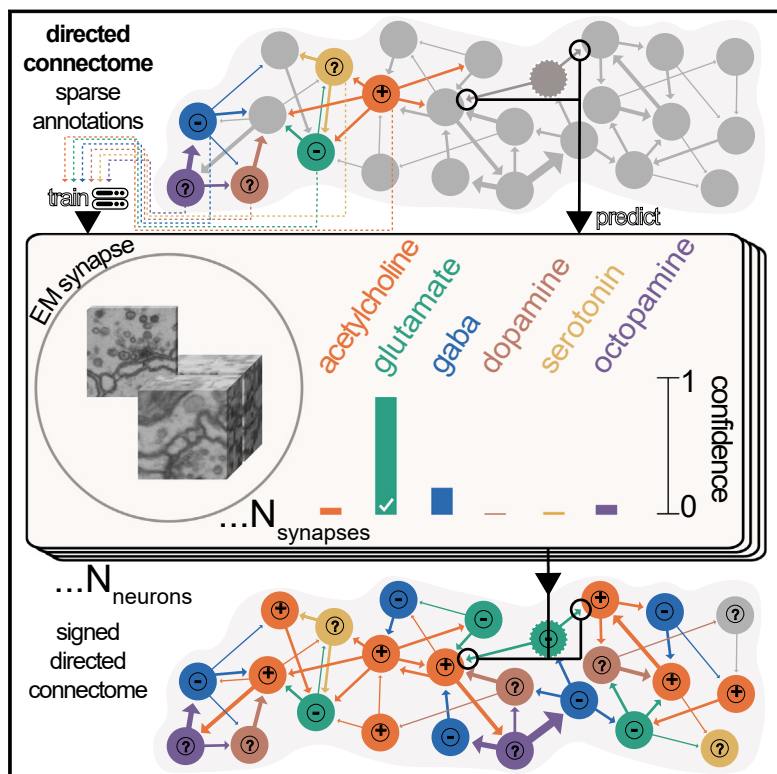


Neurotransmitter classification from electron microscopy images at synaptic sites in *Drosophila melanogaster*

Graphical abstract



Authors

Nils Eckstein, Alexander Shakeel Bates, Andrew Champion, ..., Volker Hartenstein, Gregory S.X.E. Jefferis, Jan Funke

Correspondence

funkej@janelia.hhmi.org (J.F.), jefferis@mrc-lmb.cam.ac.uk (G.S.X.E.J.)

In brief

Neurotransmitter identities are predicted directly from electron micrographs with high fidelity across the whole fly brain for acetylcholine, glutamate, GABA, dopamine, serotonin, and octopamine.

Highlights

- Machine learning identifies synaptic transmitters from electron micrographs
- Six transmitters predicted across the whole fly brain connectome
- Explainable AI reveals ultrastructural differences between transmitter identities
- Fly brain hemilineages predominantly express one fast-acting transmitter



Resource

Neurotransmitter classification from electron microscopy images at synaptic sites in *Drosophila melanogaster*

Nils Eckstein,^{1,2,9} Alexander Shakeel Bates,^{3,4,5,9} Andrew Champion,⁶ Michelle Du,¹ Yijie Yin,⁶ Philipp Schlegel,^{3,6} Alicia Kun-Yang Lu,¹ Thomson Rymer,¹ Samantha Finley-May,¹ Tyler Paterson,¹ Ruchi Parekh,¹ Sven Dorkenwald,⁷ Arie Matsliah,⁷ Szi-Chieh Yu,⁷ Claire McKellar,⁷ Amy Sterling,⁷ Katharina Eichler,⁶ Marta Costa,⁶ Sebastian Seung,⁷ Mala Murthy,⁷ Volker Hartenstein,⁸ Gregory S.X.E. Jefferis,^{3,6,*} and Jan Funke^{1,10,*}

¹HHMI Janelia Research Campus, Ashburn, VA, USA

²Institute of Neuroinformatics UZH/ETHZ, Zurich, Switzerland

³Neurobiology Division, MRC Laboratory of Molecular Biology, Cambridge, UK

⁴Centre for Neural Circuits and Behaviour, The University of Oxford, Tinsley Building, Mansfield Road, Oxford OX1 3SR, UK

⁵Department of Neurobiology and Howard Hughes Medical Institute, Harvard Medical School, Boston, MA, USA

⁶Drosophila Connectomics Group, Department of Zoology, University of Cambridge, Cambridge, UK

⁷Princeton Neuroscience Institute, Princeton University, Princeton, NJ, USA

⁸Department of Molecular Cell and Developmental Biology, University of California, Los Angeles, Los Angeles, CA, USA

⁹These authors contributed equally

¹⁰Lead contact

*Correspondence: funkej@janelia.hhmi.org (J.F.), jefferis@mrc-lmb.cam.ac.uk (G.S.X.E.J.)

<https://doi.org/10.1016/j.cell.2024.03.016>

SUMMARY

High-resolution electron microscopy of nervous systems has enabled the reconstruction of synaptic connectomes. However, we do not know the synaptic sign for each connection (i.e., whether a connection is excitatory or inhibitory), which is implied by the released transmitter. We demonstrate that artificial neural networks can predict transmitter types for presynapses from electron micrographs: a network trained to predict six transmitters (acetylcholine, glutamate, GABA, serotonin, dopamine, octopamine) achieves an accuracy of 87% for individual synapses, 94% for neurons, and 91% for known cell types across a *D. melanogaster* whole brain. We visualize the ultrastructural features used for prediction, discovering subtle but significant differences between transmitter phenotypes. We also analyze transmitter distributions across the brain and find that neurons that develop together largely express only one fast-acting transmitter (acetylcholine, glutamate, or GABA). We hope that our publicly available predictions act as an accelerant for neuroscientific hypothesis generation for the fly.

INTRODUCTION

Generating a synaptic connectome entails identifying all neurons and synapses in a sample. Recent advances in volume electron microscopy (EM) have enabled connectome generation for entire nervous systems.^{1–6} Automated methods for segmenting neurons,^{7–11} detecting synapses,^{12–16} and proofreading¹⁷ have significantly reduced the human effort required. These methods have been applied to create connectomes for the *Drosophila melanogaster* brain^{6,18,19} and its ventral nerve cord.^{5,20} However, EM does not directly tell us about gene expression, most crucially the transmitter pathways active in each neuron. This gap hinders our understanding of key neurobiological processes relevant to circuit function.

The action that a neuron has on its downstream targets depends on the transmitter it releases and the postsynaptic recep-

tors that receive it. The so-called *classical* fast-acting transmitters (i.e., acetylcholine, glutamate, and GABA) are most common.^{21,22} They are contained in small, clear vesicles. Monoamines such as dopamine, serotonin, and octopamine are packaged into clear core or small dense core vesicles.²³ About 53 neuropeptides and peptide hormones^{24–26} are contained in larger dense core vesicles.^{27,28} While co-transmission of a small molecule transmitter and a neuropeptide is common,^{21,22,29} the usage of acetylcholine, glutamate, and GABA is largely mutually exclusive.^{30,31} Therefore, Dale's law, an expectation that each neuron expresses a single small molecule transmitter, often guides our hypotheses about neuronal function.^{32,33} We expect that this transmitter expression will be stereotyped for cell types across individuals, given their shared gene expression profiles.³⁴ We also expect transmitter expression to be organized at higher levels, for example by hemilineage. Hemilineages are basic



developmental units of the insect brain and typically consist of dozens of cell types. In the ventral nerve cord Lacin et al.³¹ comprehensively showed that only one of acetylcholine, glutamate, or GABA is expressed per hemilineage. By analogy with Dale's law, we call this observation Lacin's law. It was unclear whether Lacin's law also holds in the brain.

In larger organisms, experts can distinguish excitatory and inhibitory transmitters based on synaptic vesicle ellipticity^{35–37} or synapse symmetry.³⁸ However, in invertebrates transmitter identity cannot be consistently identified by human annotators from electron micrographs. Instead, investigators use molecular biology and light microscopy pipelines to link RNA expression data or immunoreactivity to proteins involved in transmitter biosynthesis with specific neuronal morphologies.^{22,39–44} Standard high-throughput methods such as single-cell RNA-seq cannot be used since they do not retain morphology information. Therefore, researchers profile sparse genetic driver lines,^{45,46} which target only a few neurons, followed by accurate morphological matching to EM reconstructions.^{47,48} Since these experimental pipelines can take weeks per cell type and are limited by the availability of sparse genetic driver lines, they do not scale to whole nervous system discovery. Consequently, the transmitter identity is known for only ~700 of the ~7,000 cell types of the adult *D. melanogaster* central brain.^{49,50} However, this subset provided ground truth that we can use to learn the features of specific transmission types, by mapping known transmitter identities to previously localized presynaptic sites in two brain datasets (FAFB [the Full Adult Fly Brain]⁶ and the HemiBrain⁵¹).

RESULTS

Assembling ground-truth neurotransmission data

We compiled a list of 356 *D. melanogaster* neuronal cell types from 21 studies (Data S1), selecting those with robust transmitter data. We identified these same cell types within the FAFB-Catmaid and HemiBrain datasets (Figure 1A). We selected cell types with clear transmitter data from RNA expression or immunohistochemistry, complemented by specific cell type targeting through the GAL4/split-GAL4 system.⁴⁶ We did not generally pursue types reported to exhibit co-transmission (see STAR Methods). Given that *D. melanogaster* neurons are highly stereotyped,⁵⁰ these cell types were identifiable in our EM datasets. We chose to proceed with transmitters supported by at least 10 EM reconstructions per dataset, i.e., acetylcholine, glutamate, dopamine, serotonin, and octopamine (Data S1, see STAR Methods). All presynapses for each neuronal reconstruction were assumed to use the single small-molecule transmitter reported in the literature (Figure 1B). In total, we matched 3,025 FAFB-Catmaid neuronal reconstructions (211,564 synapses) and 5,902 HemiBrain reconstructions (840,535) to cell types with a known transmitter (Data S2).

We took a slightly different approach in selecting presynapses from our two datasets. For HemiBrain, we used automatically predicted presynaptic sites across many brain cell types, of which a proportion are false detections.¹³ In FAFB, however, we used manually placed synaptic markers laid by human researchers from a smaller pool of manually reconstructed neurons (see STAR Methods). Therefore, compared with

HemiBrain, our FAFB-Catmaid dataset contained higher-quality synapses from a smaller number of neurons. Note that in later results, to work with the full connectome, we explored transmitter predictions across automatically detected presynapses¹² in the newer FAFB-FlyWire reconstruction project.^{17,18,50} After building our ground truth, we expanded our literature review to find 268 more cell types with the reported transmission of one of our six transmitters (Data S7), which we could use to further validate our results.

Network architecture, training, testing, and validation datasets

For each transmitter $y \in \{\text{GABA, acetylcholine, glutamate, serotonin, octopamine, dopamine}\}$, we partitioned the data into training, testing, and validation sets by randomly assigning entire neurons (neuron split), such that approximately 70% of presynapses were used for training, 10% for validation, and the remaining 20% for testing. This approach mirrors real-world scenarios where we typically know the transmitter of an entire neuron and are interested in predicting the transmitter of a different neuron. We employed a 3D deep convolutional network based on the Visual Geometry Group (VGG) architecture⁵² to predict transmitter identity from cubes of EM image data (edge length 640 nm), each centered on a presynaptic site (Figure 1C). The cube size was chosen to be large enough to provide surrounding context, including synaptic features like vesicles, T-bars, clefts, and postsynaptic densities, while at the same time being small enough to fit into the limited memory of a GPU. The network consisted of four functional blocks, each with two 3D convolution operations, batch normalization, ReLU non-linearities, and subsequent max pooling with a downsampling factor of 2, except for FAFB where we limited downsampling to the x and y dimensions for the first three blocks to account for image voxel anisotropy. The last block was followed by three fully connected layers with dropout ($p = 0.5$) applied to the last one. We trained the network to minimize cross-entropy loss over the six classes (GABA, acetylcholine, glutamate, serotonin, octopamine, and dopamine) using the Adam optimizer.⁵³ We trained for a total of 500,000 iterations in batches containing eight samples and selected the iteration with the highest validation accuracy for testing.

For the FAFB neuron split, the testing set consisted of a total of 40,104 presynapses from 185 neurons that the network was not trained on. The network achieved an average per-transmitter accuracy of 87% on FAFB and 78% on HemiBrain. We assigned each neuron with over 30 presynapses in the testing set a transmitter through a majority vote of its presynapses, yielding an average accuracy of 94% for transmitter prediction per neuron on FAFB-Catmaid and 91% on HemiBrain (Figure 2A). Our goal was to train a network with high prediction accuracy based on ultrastructural features of synapses. Cytological correlates of synapse location or neuron development might have driven transmitter identification by our network. We, therefore, split the data by the neuropil (i.e., brain region) location of synapses⁵⁴ (Figure 2B) and their developmental origin (hemilineage) (Figure 2C). Accuracy in these split datasets remained high (Figure 1D), indicating that the network is unlikely to use related features.

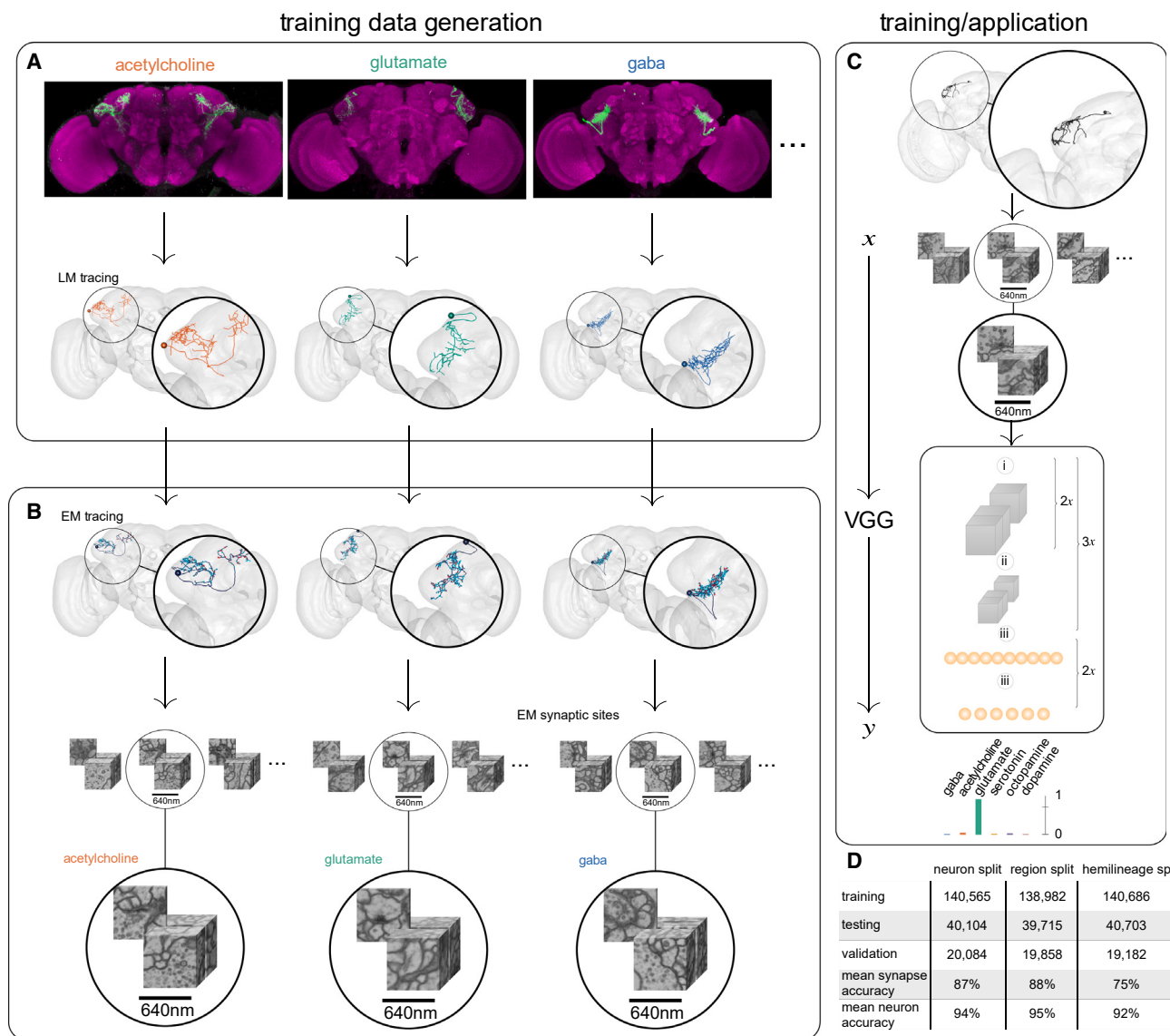


Figure 1. Method overview

We assembled a dataset of neurons with known transmitter expression (see [STAR Methods](#)) in two *D. melanogaster* brain EM datasets (FAFB and HemiBrain) and retrieved corresponding synaptic locations.

(A) Typically, neurons had been genetically tagged to identify their transmitter identity and reconstruct their coarse morphology using light microscopy ([Data S1](#)).

(B) Light microscopy tracings of neurons are then matched to corresponding EM reconstructions with annotated synaptic locations, yielding a dataset of EM volumes of synaptic sites with known transmitter identity.

(C) We used the resulting pair (x, y) where x is a 3D EM volume of a synaptic site and y is the transmitter of that synaptic site (one of GABA, acetylcholine, glutamate, serotonin, octopamine, or dopamine) to train a 3D VGG-style deep neural network to assign a given synaptic site x to one of the six considered transmitters. We used the trained network to predict the transmitter identity of synapses from neurons with so far unknown transmitter identity. Panels i, ii, and iii denote convolution, down-sampling, and fully connected layers, respectively.

(D) Overview of our results on the FAFB dataset. Shown are the number of presynapses for training, testing, and validation as well as average synapse and neuron classification accuracy on the testing set for each data split.

See also [Data S2](#).

Applying Dale's law to the entirety of both datasets, we adopted the most frequent synapse-level transmitter prediction as the neuron-level transmitter prediction and developed a confidence score based on the proportion of presynapses that "voted" for the neuron-level transmitter prediction and our confusion

matrices (see [STAR Methods](#)). The distribution of confidence scores across the two datasets suggested the network was most confident in acetylcholine predictions ([Figure 2D](#)). In general, we found excellent agreement with the literature ([Data S7](#)). We predicted most known cholinergic cell types correctly

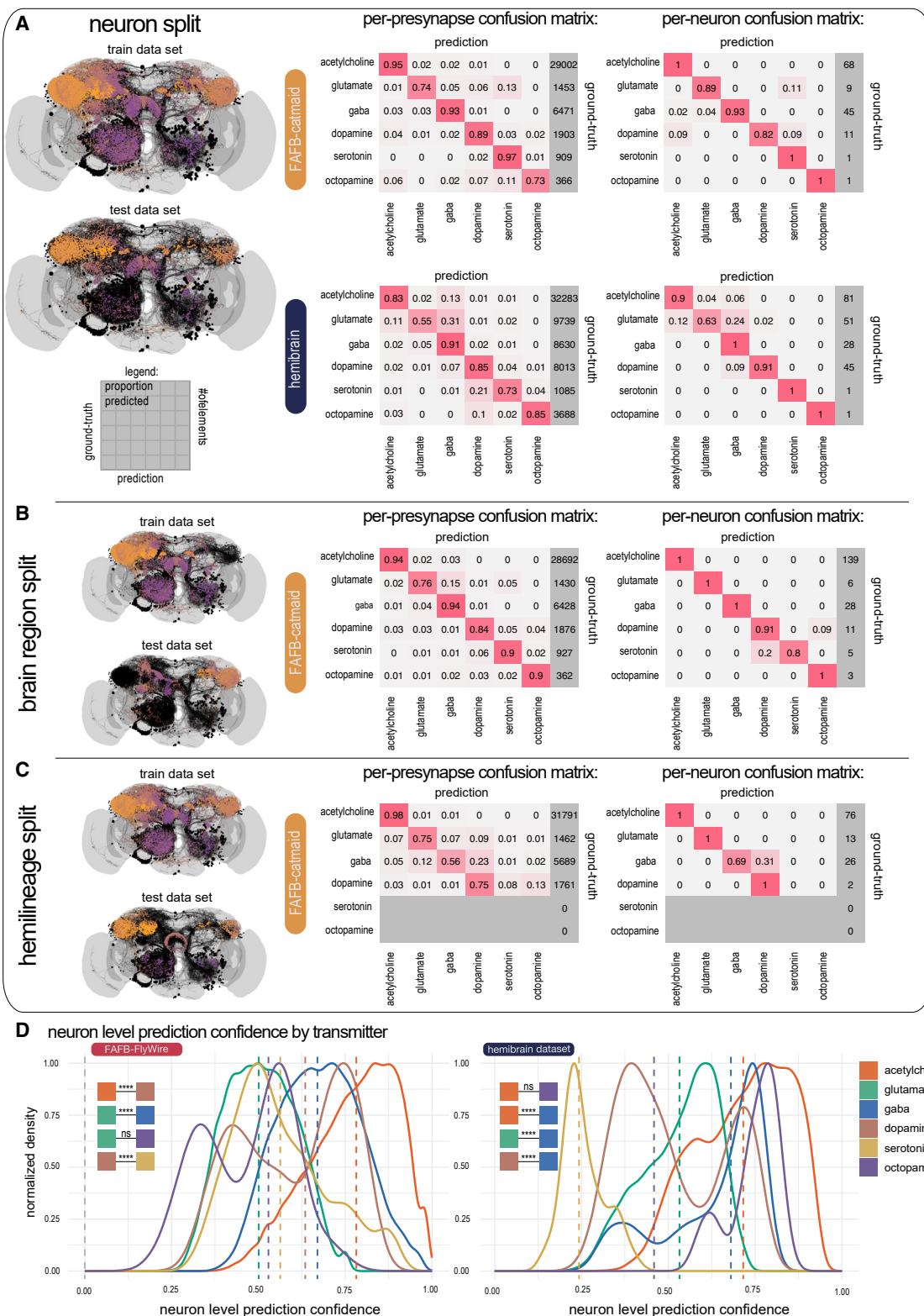


Figure 2. The accuracy of the trained classifier on a per-presynapse and per-neuron basis

(A) Left: visualization of the training (upper) and testing (lower) data (split by entire neurons) that we used for the results in this manuscript. Presynapse locations are color coded according to their z-depth; anterior-posterior shown as purple-orange, neuron skeletons in black. Right: confusion matrices for the trained

(legend continued on next page)

(FAFB-FlyWire, 91%; HemiBrain, 91%), as well as most glutamatergic (FAFB-FlyWire, 91%; HemiBrain, 95%), GABAergic (FAFB-FlyWire, 96%; HemiBrain, 97%), dopaminergic (FAFB-FlyWire, 90%; HemiBrain, 85%), and octopaminergic (FAFB-FlyWire, 85%; HemiBrain, 100%) cell types (Figures S2D and S2F). Notably, the optic lobe, which has the most known transmitter assignment,³⁹ was largely not used in our ground truth due to a relative paucity of FAFB-Catmaid reconstructions and its absence from the HemiBrain dataset. Nevertheless, 96% of ~29,000 cholinergic optic lobe neurons were predicted correctly, as well as 87% of ~3,600 GABAergic neurons and 91% of ~1,600 glutamatergic neurons.

However, we noticed a few clear mispredictions and discrepancies, most commonly in cases of suspected co-transmission (see STAR Methods). For example, Kenyon cells had been mispredicted for dopamine in both HemiBrain and FAFB-FlyWire rather than acetylcholine,⁵⁵ some known serotonergic neurons (Figure S2E) were not predicted for serotonin in either dataset,^{56–60} many first-order sensory neurons and antennal lobe local neurons were mispredicted for serotonin rather than acetylcholine in both datasets^{61–64} and some intrinsic neurons of the fan-shaped body were mispredicted in HemiBrain but not in FAFB-FlyWire and vice versa. Overall, serotonin was our least reliable prediction (FAFB-FlyWire, 33%; HemiBrain, 38%) likely due to its relative paucity in our ground-truth data. Our results for a full ventral nerve cord (MaleVNC, 82% accuracy, limited to acetylcholine, glutamate, and GABA) are reported elsewhere.^{5,65}

Classifier synapse feature analysis

The classifier's high accuracy on test datasets raised questions about how transmitter classes are discriminated, as human annotators cannot reliably determine transmitter identity from EM alone. We reasoned that identifying the visual features that our network used to label transmitters could verify that decisions were not based on class-irrelevant confounders and discover unknown ultrastructural differences between synapse classes. To visualize these features, we explored *post hoc* single-input attribution methods that derive an attribution map for a single input image, highlighting image areas crucial for classification. Existing methods^{66–69} did not provide images we could interpret since the highlighted areas were too large and variable. This may be because single-input attribution methods are subject to highlighting non-class-specific "distractors,"⁷⁰ e.g., features stemming from different orientations of the synapse, section thickness, or intensity variations. We introduced an attribution method to focus on class-relevant features between pairs of classes while disregarding distractors⁷¹ and used the FAFB da-

taset for its superior x,y resolution. Given a real image x_R of a class y_R , we first created a counterfactual image x_C by translating x_R into an image of another class y_C using a CycleGAN,⁷² resulting in paired images of different transmitter types. Crucially, this domain translation of an image from class y_R to class y_C keeps class-irrelevant distractors (e.g., the orientation of the synapse) intact. Class-relevant features, however, are changed due to the adversarially trained discriminator of the CycleGAN. We used our previously trained classifier to confirm that the domain translation was successful: we filtered all images such that x_R was classified as y_R and the counterfactual x_C as y_C . We then identified a small region in x_C , that when swapped with x_R changed the prediction of the trained classifier (Figures 3A and 3B). Specifically, we identified a minimal binary mask m , such that the hybrid image $x_H = m \cdot x_R + (1 - m) \cdot x_C$ was classified as y_R . To find m , we used a modified version of the DeepLift method, where we used the counterfactual x_C as the neutral ref.⁷¹

This method allowed us to manually identify at least one distinguishing feature (Figure 3C) between each pair of transmitters (see Data S8). We only included features consistently observed in both directions, e.g., translating a real GABA image to acetylcholine results in a brighter cleft and translating a real acetylcholine image to GABA produces a darker cleft. Comparing transmitter identities in paired images allowed us to observe features as subtle as sub-pixel changes in vesicle diameters (e.g., between GABA and glutamate), which would be near impossible to pick up in unpaired images. We confirmed the identified features between the classical transmitters GABA, acetylcholine and glutamate on the original synapse images by manually segmenting the synaptic cleft, vesicles, and T-bars of 222 synapse images (75 GABA, 85 acetylcholine, 62 glutamate; annotators were blind to the predicted transmitter class). We found strong support for each of the identified features between those transmitters (Figures 3D–3F): acetylcholine has a brighter cleft than GABA and glutamate ($p \leq 0.0001$), glutamate has larger vesicles than GABA ($p \leq 0.001$) and glutamate has a darker T-bar than acetylcholine ($p \leq 0.001$).

Comparing neurotransmitter predictions for neuron homologs across datasets

The insect brain consists of thousands of isomorphic cell types. Every cell type has a copy on each hemisphere. These cell types contain only a few neurons (median, 2, IQR, 2, neurons per cell type per hemisphere for the HemiBrain dataset, excluding the largest outlier classes of Kenyon cells and sensory receptor neurons), often only a single neuron per hemisphere (41% of cell types in HemiBrain). We refer to these neurons as singletons.

classifier on the testing data, shown per presynapse and as a majority vote per neuron, on datasets FAFB and HemiBrain. We considered only those neurons with more than 30 presynapses.

(B) Classification results on alternative training and testing data (split by brain regions) from FAFB.

(C) Same as (B) but split by hemilineage. It was not possible to generate a fully balanced split and as a result there are no serotonin and octopamine neurons in the testing set, as indicated by the grayed-out rows.

(D) The distribution of neuron-level confidence scores by transmitter, across our pool of central brain neurons in the FlyWire and HemiBrain datasets (FAFB-FlyWire, 136,927; HemiBrain, 24,666). Vertical dashed line, median value. Colored boxes with stars indicate statistical comparisons, Wilcoxon two-sample tests (n.s., not significant; * $p \leq 0.05$; *** $p \leq 0.00001$).

See also Figure S1 and Data S3 and S4.

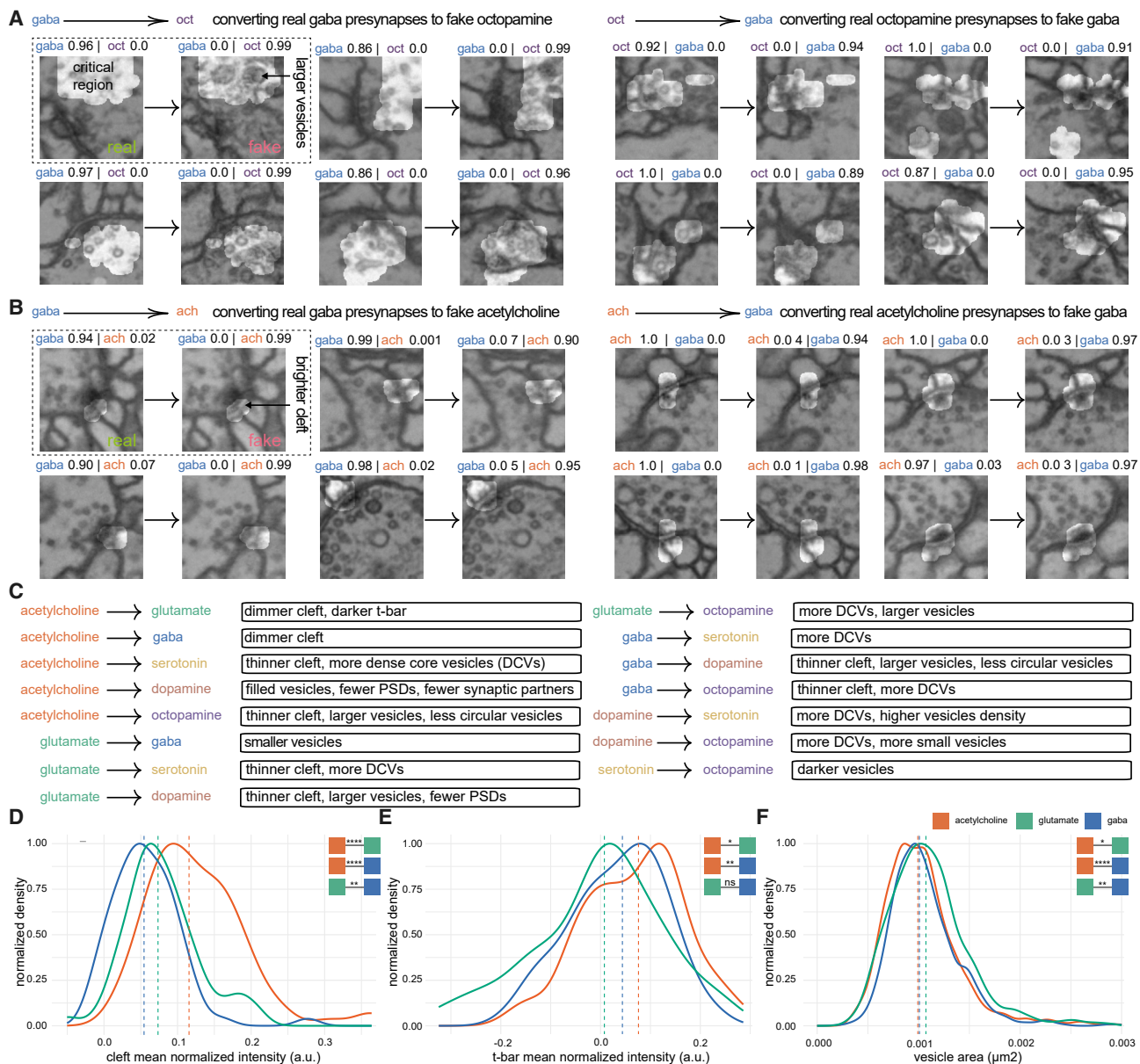


Figure 3. Classifier feature analysis using a discriminative attribution method

- (A) Example translations of real synapse images to fake counterfactual images. Highlights show attribution masks indicating the most important changes between the two classes. Classifier scores are shown above each image. Left, two columns show the translation of real GABA synapses into counterfactual octopamine synapses. Right, same as left but for octopamine to GABA.
- (B) Same as (A) but for GABA-acetylcholine.
- (C) Pairwise differences between transmitters, found through manual inspection of real and counterfactual images. Dense core vesicles, DCVs; postsynaptic densities, PSDs.
- (D) Normalized density plot showing the distribution of cleft intensity among original synapse images. Number of annotated synapses: acetylcholine 84, glutamate 61, GABA 74.
- (E) Same as (C) for T-bar intensities. Number of annotated synapses: acetylcholine 85, glutamate 62, GABA 75.
- (F) Same as (C) for vesicle sizes. Number of annotated vesicles: acetylcholine 1,729, glutamate 1,153, GABA 1,382. Vertical dashed line, median value. Colored boxes with stars indicate statistical comparisons, Wilcoxon tests. Note that the vesicle size comparison assumes that vesicle sizes from the same synapses are conditionally independent given the transmitter (n.s., not significant; $*p \leq 0.05$; $**p \leq 0.001$; $***p \leq 0.00001$).

See also Figure S1 and Data S8.

They provide a natural mechanism by which to test whether our transmitter predictions are consistent as, being unique on each hemisphere, they can be unambiguous matching to their homologs between hemispheres and brains (Figure 4A). We matched 1,586 right hemisphere singletons to their left hemisphere homologs in FAFB-FlyWire and 1,318 to their HemiBrain homologs.⁵⁰

We found good agreement between left-right matched FAFB-FlyWire singletons (Figure 4B) and FAFB-HemiBrain matched singletons (Figure 4C) for cholinergic, glutamatergic, and GABAergic pairs. Inconsistent results between matched neurons were more common with singletons predicted to express dopamine, serotonin, or octopamine. The average confidence score for FAFB-FlyWire right (mean, 0.79, SD, 0.16), FAFB-FlyWire left (mean, 0.79, SD, 0.17), and HemiBrain (mean, 0.67, SD, 0.14) neurons were significantly higher when there was no mismatch between our paired neurons than when there was a conflict (FAFB-FlyWire right: mean, 0.62, SD, 0.22; FAFB-FlyWire left: mean, 0.47, SD, 0.14; hemibrain: mean, 0.43, SD, 0.13) (Figure 4D).

We found that matched singleton pairs and cell types correlated in their neuron-level transmitter prediction scores (Figures 4D–4F and S2A). When the network was less confident it was consistently less confident for both members of a pair, both across hemispheres and datasets, although within-dataset comparisons were more similar (Figure 4E). In cases where changes in the confidence score were correlated, the reason is more likely to be biological than dataset specific. For example, low, correlated scores could indicate that the network has encountered a biological situation that is rare in, or outside of, our training data.

We also examined isomorphic cell types in the HemiBrain dataset for which there was more than one member of the cell type per hemisphere (Figures 4F and S2B). Only 14% of cell types with more than one member per hemisphere did not have the same neuron-level transmitter prediction for each member. Moreover, we matched 2,626 neuronal cell types between FAFB-FlyWire and the HemiBrain datasets and found that 95% agree in their neuron-level transmitter prediction between the two datasets (Figures S2B and S2C). Again, among these conflicted types, the mean neuron-level transmitter prediction score was significantly lower (Figure S2C). Together, this suggests that there may be a biological factor, e.g., the expression of transmitters not in our training data or co-transmission, that leads to lower confidence scores and incorrect or inconsistent predictions with certain cell types, rather than a confound related to the EM data quality.

An overview of neurotransmitter usage in the nervous system

We next wanted to get an overview of transmitter usage in the *D. melanogaster* nervous system (Figures 5A and 5B), including a breakdown by axon and dendrite connections across the brain (Figures 5C, 5D, and 6B). We also explored potential correlations between neuron-level morphological features and transmitter predictions (Figures 5E, 5F, and S3), alongside variations in transmitter usage across sensory systems within the fly brain (Figure 6A).

We calculated neuron-level transmitter predictions for all 24,666 well-reconstructed neurons in the HemiBrain dataset (Data S3), all 49,985 central brain and 86,942 optic lobe FAFB-FlyWire neurons (Data S4), and 23,503 ventral nerve cord neurons from the MaleVNC dataset. In the central brain, the largest fraction of neurons were predicted to be cholinergic with smaller fractions for glutamatergic and GABAergic neurons (Figure 6A). Single-cell RNA sequencing has suggested a breakdown of 44%–45% cholinergic, 14%–15% glutamatergic, and 10%–15% GABAergic neurons^{21,22} in the central brain. Dopaminergic neurons had distinctive features, such as higher mitochondrial density (Figure S3C), a diverse set of input neurons but fewer downstream targets (Figure S3I), primarily in deeper sensory layers (Figure 6C). They are encountered after Kenyon cells in the olfactory system (often thought of as a conditioned stimulus) but before the mushroom body in the gustatory system (typically an unconditioned stimulus). These observations suggest that dopaminergic neurons are highly active and sample widely from more superficial brain layers to provide teaching signals to select target neurons of a deeper sensory layer.

One interesting new insight from large-scale neuron-level transmitter predictions concerns the fan-shaped body. This central brain structure computes navigational variables^{75,76} and is built as a matrix with ~9 rows and ~10 columns.⁷⁷ Our predictions show that row-wise tangential input is overwhelmingly glutamatergic (~84%), with no inhibitory local neurons in the structure. There are some dopaminergic⁷⁸ but very few GABAergic or cholinergic row-wise inputs. In contrast, acetylcholine was predicted for almost all column-wise input types (~87%), intrinsic neurons (~88%), and output types (~96%); the small number of non-cholinergic neurons are likely mispredictions (see STAR Methods). These findings can be compared to the elegant layout of transmitter expression in the mushroom body,⁷⁹ a discovery that has accelerated research in this associative memory structure in recent years.

The identity of the presynaptic and postsynaptic neuronal compartments is another factor, in addition to transmitter usage, that determines the effect of a synaptic connection.⁸⁰ Insect neurons frequently possess arbor with a mix of input and output synapses, but morphological features can resolve axons and dendrites in most cases^{19,73,74,81–83} (Figure 5C). Axons and dendrites can synaptically connect with either being the source or the target (Figures 5C and 5B). We “split”⁷³ thousands of neurons into separate axonal and dendritic compartments (see STAR Methods). Although most presynapses are on the axon (FAFB-FlyWire: median 76%, SD, 21%; hemibrain: median 70%, SD, 21%), neurons had a large proportion of their output sites on their dendrites (FAFB-FlyWire: median 23%, SD, 21%; hemibrain: median 30%, SD, 21%). We found that while the majority of the synaptic budget is spent on axo-dendritic connections (FAFB-FlyWire: 55%; hemibrain: 48%), a large fraction is spent on axo-axonic connections (FAFB-FlyWire: 22%; Hemi-Brain: 20%) and a similar amount on dendro-dendritic connections (FAFB-FlyWire: 19%; hemibrain: 21%). These figures are comparable to those recently reported for the *D. melanogaster* larva¹⁹ (axo-dendritic, 54%; axo-axonic, 36%; dendro-dendritic, 8%; dendro-axonic, 3%). Neurons tended to receive strong input on their axons from just one of acetylcholine, glutamate,

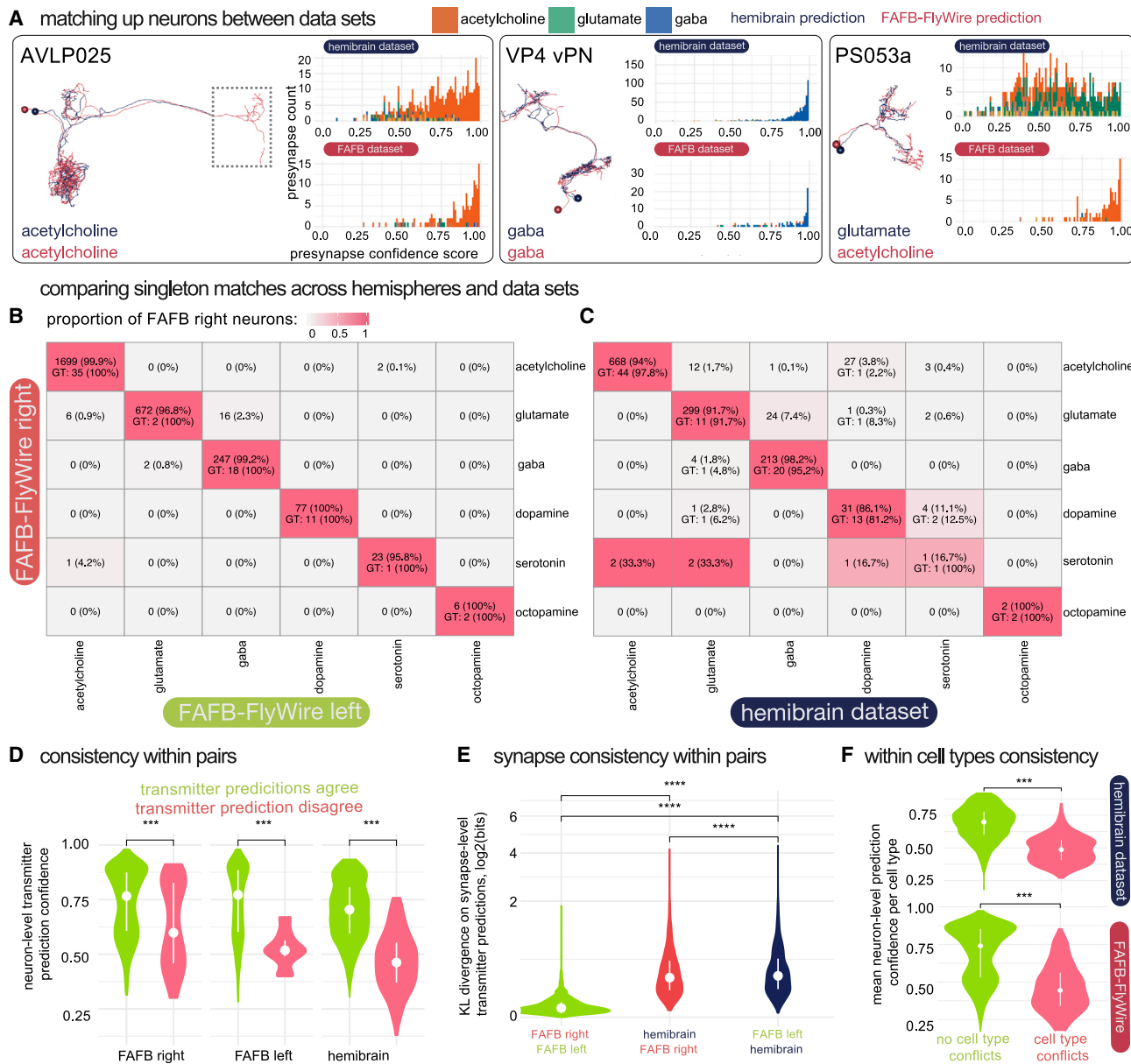


Figure 4. Comparing neuron-level transmitter predictions between connectome datasets from separate animals and between hemispheres

(A) Images of co-registered, matched neurons between the HemiBrain (navy) and the FAFB-FlyWire (red) datasets. Histograms show synapse-level transmitter prediction scores for exemplar pairs. Neurons can be matched despite missing data (left, grey dashed box). PS053a has conflicting neuron-level transmitter predictions.

(B) Confusion matrix compares matched singleton FAFB-FlyWire-right and FAFB-FlyWire-left pairs' neuron-level transmitter predictions (1,586 pairs).

(C) Confusion matrix comparing matched FAFB-FlyWire-right and HemiBrain-right neuron-level transmitter predictions (1,318 pairs). Cells colored by the proportion of FAFB-FlyWire right neurons of each transmitter type (row normalized) that are matched to its homolog-columns give homolog prediction.

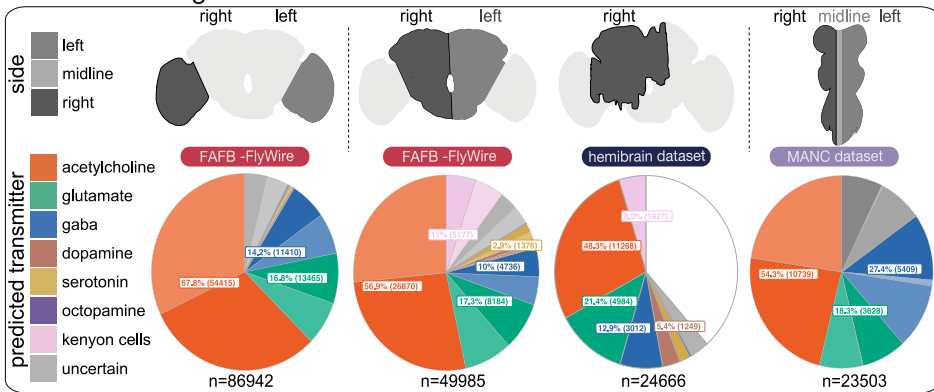
(D) Neuron-level transmitter prediction scores between matched singletons that have (red, right) or do not have (green, left) a conflict between their neuron-level transmitter predictions, across all three hemispheres. Matches:mismatches across all comparisons for FAFB-FlyWire right: 2,650:170 FAFB-FlyWire left, 1,562:40, and HemiBrain neurons, 1,088:130.

(E) Comparison of similarity scores for matches (Kullback-Leibler divergence on synapse-level transmitter prediction scores).

(F) The neuron-level transmitter prediction consistency among cell types that have multiple repeats, i.e., not singletons. Green, the mean neuron-level transmitter prediction confidence for cell types where all members of the type are predicted to use the same transmitter. Red, the mean neuron-level transmitter prediction confidence for cell types where not all members of the type are predicted to use the same transmitter. Violin plots show the median value (dot) and the interquartile range (line, 25th to 75th percentiles). Data were compared using Wilcoxon two-sample tests (n.s., not significant; ***p ≤ 0.0001; ****p ≤ 0.00001).

See also Figure S2 and Data S7.

A transmitter usage breakdown



C axon-dendrite split

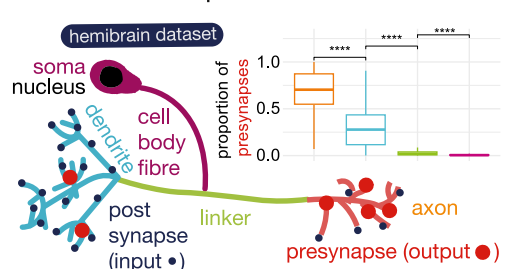


Figure 5. Breakdown of transmitter use across the *D. melanogaster* nervous system

(A) Our neuron-level transmitter predictions across the female optic lobes and central brain and a male ventral nerve cord (see STAR Methods).

(B) Bar plots for the numbers of neurons predicted for different transmitter usages in each super class in the FAFB-FlyWire dataset.⁵⁰

(C) Schematic of a neuron broken into its neuronal compartments. Inset, the proportion of presynapses in each of the four compartment types.

(D) Synaptic budget across different connection types in FAFB-FlyWire (left) and HemiBrain (right). Heatmaps show the proportion of synaptic contacts from neurons of different predicted transmitter types (columns) used in different inter-compartmental connection types (rows). FAFB-FlyWire, 9,123; hemibrain, 10,122 neurons.

(E) Scaled density plots showing neuronal polarity by neuron-level transmitter prediction. Upper, distribution of projection scores, which is the distance in Euclidean space between the dendritic and axonic midpoint. Lower, segregation index: the higher the score, the more polarized the neuron.⁷³

(F) Scaled density plots showing the distribution of excitation-inhibition balance (proportion of excitatory, acetylcholine, input minus the proportion of inhibitory input; GABA, glutamate) across neuron-level transmitter predictions and compartments. Vertical dashed line, median value. Colored boxes with stars indicate statistical comparisons, Wilcoxon two-sample tests (n.s., not significant; * $p \leq 0.05$; ** $p \leq 0.0001$; *** $p \leq 0.00001$).

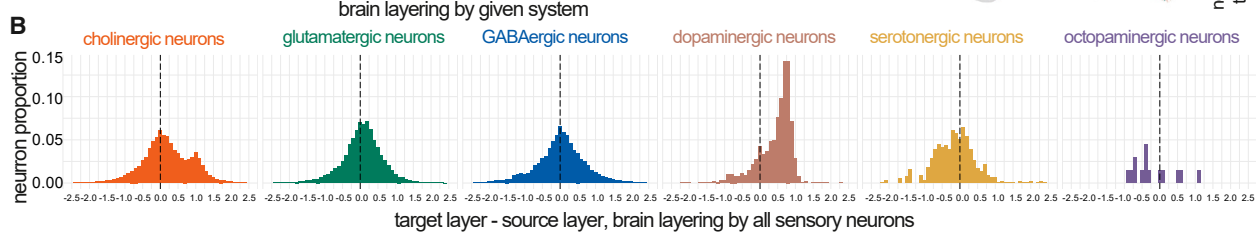
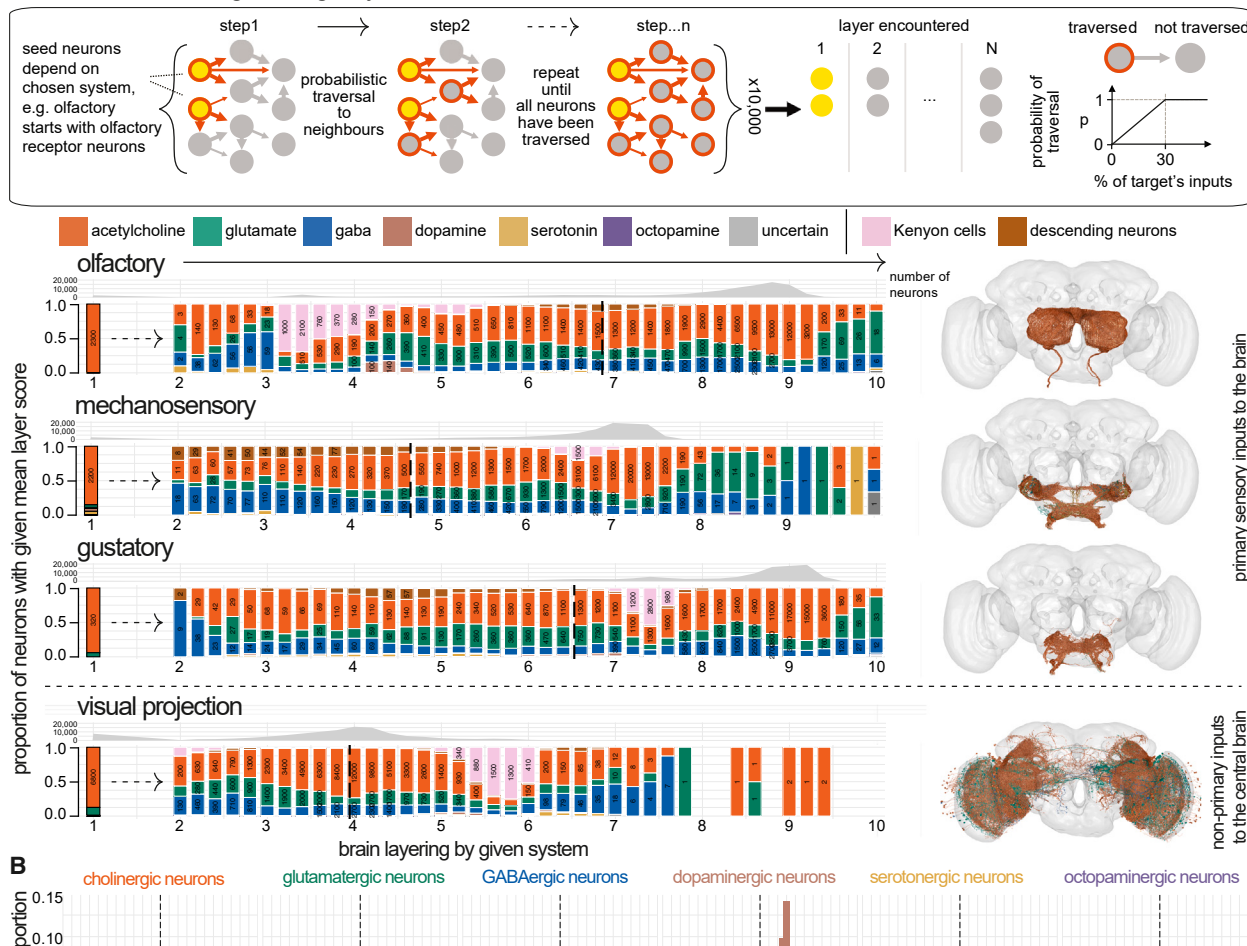
See also Figures S2 and S3 and Data S3 and S4.

or GABA (Figure S4A), in patterns that were consistent between the two datasets (Figure S4B, cosine similarity > 0.9). Axons may therefore be particularly selective in their inputs, particularly inhibitory inputs (Figure S3E).

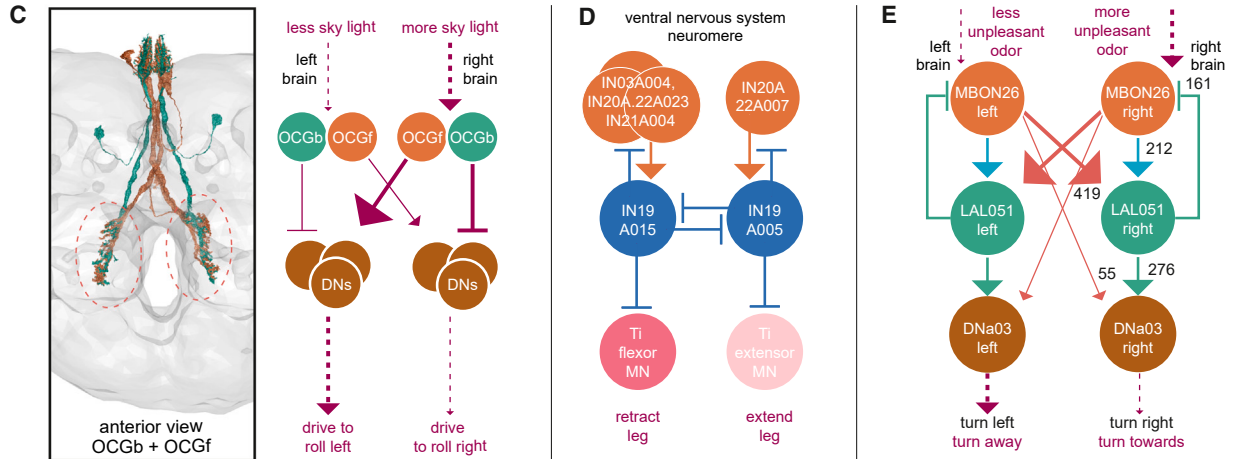
Comparing putative inhibitory and excitatory neurons

Putative excitatory neurons predominate in the brain (Figure 5A). The principal excitatory transmitter is acetylcholine,^{84,85} and the main inhibitory transmitter is GABA.^{86–88} Glutamate can act in

A transmitter usage through layers of the brain FAFB-FlyWire



examples insight using predicted transmitters



(legend on next page)

either an inhibitory^{89–92} or excitatory capacity.^{93–95} Analyzing the FAFB-FlyWire dataset using a probabilistic layer assignment model,^{18,74} we observed shifts in the proportions of transmitter use across sensory systems. For example, there is a greater proportion of GABAergic neurons in the early olfactory system, with glutamatergic neurons rising later. This switch also suggests that neurons in deeper layers are likely to be inhibited by glutamate because GABA is scarce.

Cholinergic (mean 0.21, SD, 0.75) and glutamatergic (mean 0.07, SD, 0.57) neurons tended to target higher-layer neurons (Figure 6B) i.e., predominantly feedforward connectivity; GABAergic neurons had no such bias (mean –0.02, SD, 0.61). On average, GABAergic neurons were more “local” in Euclidean space than cholinergic neurons (Figure 5E upper); they were also smaller by cable length (Figure S3A) and less polarized (Figure 5E lower). However, on average GABAergic neurons had more input neurons and downstream targets (Figure S3I). These connections may have a stronger effect than their cholinergic counterparts for two reasons; first, they show greater synaptic count (Figure S3F), and second, because they are located slightly closer to the target neuron’s primary branch point (Figure S3H), which could enable more powerful inhibition.⁹⁶ Additionally, GABAergic neurons had higher mitochondrial density than cholinergic or glutamatergic neurons (Figure S3C), which could indicate a higher level of energy use and neuronal activity. Lastly, GABAergic neurons received more excitatory than inhibitory drive onto their dendrites compared with cholinergic neurons (Figure S3E). Instead, cholinergic neurons often have large inhibitory inputs onto their axons (median, –0.16). Together, this could mean that GABAergic neurons are more active and integrate a wider array of inputs to inhibit a wider array of downstream neurons than cholinergic neurons; both their axons and dendrites make outputs but these are mainly local, perhaps inhibiting many competing elements in a local circuit.^{73,87,97,98} In particular, they may gate the output of cholinergic axons. On all these metrics, glutamatergic neurons lie between GABA and acetylcholine.

Example transmitter-dependent circuit hypotheses

Our brain-wide transmitter predictions now enable many testable circuit hypotheses. We present three examples that also illustrate how we think about potential confounds.

Ocellar righting circuit

In a vignette on ocellar circuitry by Dorkenwald et al.,¹⁸ our FAFB-FlyWire predictions strongly predicted that 12 OCG01 neurons (with extremely similar axonal morphologies) fall into three glutamatergic and three cholinergic cell types (Figure 6C). A hypothesis emerged: these neurons form pairs, each comprising one inhibitory and one excitatory neuron. For instance, OCG01b (glutamate) and OCG01f (acetylcholine) may collaborate to induce a righting reflex in response to sky-light cues during a roll. The hypothesis was strengthened by the internal control that having two FAFB hemispheres provides; the HemiBrain dataset, in which these neurons are heavily truncated, yielded misleading and likely false predictions (all glutamate).

Leg extension circuit

Cheong et al.⁹⁹ uncovered an inhibitory majority in local circuits controlling leg movement. The GABAergic interneurons IN19A were identified as key regulators, reciprocally inhibiting each other to prevent inappropriate co-contraction of opponent leg muscles. Upstream neurons were predicted cholinergic,⁵ creating a circuit architecture facilitating leg extension; a neuron such as IN21A004 could promote leg extension by inhibiting a flexor and disinhibiting a downstream extensor. In this case, it was initially unclear whether the 6 IN20A projection neurons (one per leg) were cholinergic or glutamatergic since 3/6 were predicted glutamatergic. However, all derive from the same hemilineage, which was majority predicted cholinergic. Since Lacin’s law is strongly followed in the ventral nerve cord,^{31,65} all six IN20A neurons are likely cholinergic.

Simultaneous excitatory and inhibitory control

The cholinergic, bilateral mushroom body output neuron, MBON26, is known to cause turning upon optogenetic activation¹⁰⁰ and innervates mushroom body compartments involved in innate olfactory aversion and appetitive learning.⁷⁹ It directly connects to the downstream turn-control descending neuron, DN03, and indirectly connects via a predicted glutamatergic local neuron, LAL051 (Figure 6E). If glutamate were purely inhibitory, we might expect unilateral MBON26 activation to result in both ipsi- and contralateral DN03 inhibition, with slightly more ipsi-DN03 activity and therefore an ipsilateral turn. If glutamate were purely excitatory, we might expect unilateral MBON26 activation to result in both ipsi- and contralateral DN03 activation, with slightly more contra-DN03 activity and therefore a

Figure 6. Transmitter usage through sensory layers and specific circuits

(A) Schematic depicts the probabilistic graph traversal model used to “layer” different sensory systems, adapted from Schlegel et al.,⁷⁴ underlying data from Dorkenwald et al.¹⁸ Starting from first-order central brain input neurons, we recorded the mean step (“layer”) at which each subsequent FAFB-FlyWire neuron is encountered by the simulation.¹⁸ Bar charts show transmitter input across distinguishable sensory systems.¹⁸ Bars normalized and binned by target neurons’ layer score (width 0.2); text reports neuron count. Kenyon cells are shown in pink and descending neurons, i.e., the last captured point of the sensory-motor transform in the brain, in brown so that the reader can compare layer progression between systems. Vertical line shows the mean descending neuron layer. Olfactory sensory neurons mispredicted for serotonin are corrected to acetylcholine.⁶⁴ “Uncertain” neurons (see STAR Methods) were removed from this analysis.

(B) Feedforward and feedback connectivity across sensory systems by neuron-level transmitter prediction. For each unitary neuron-neuron connection (greater than 100) between a source and target neuron, we calculated a target-source layer difference: the layer value⁷⁴ for the target neuron minus the layer value of the source neuron. Y axis gives the proportion of unitary connections in each bin (width 0.1).

(C) A potential circuit for righting the fly’s body axis relative to celestial cues. Purple arrow weight indicates activity level.

(D) A potential circuit for differential leg extension/retraction control.

(E) A potential circuit for steering away from unpleasant odors. Numbers give synaptic counts from HemiBrain.

See also Figure S4.

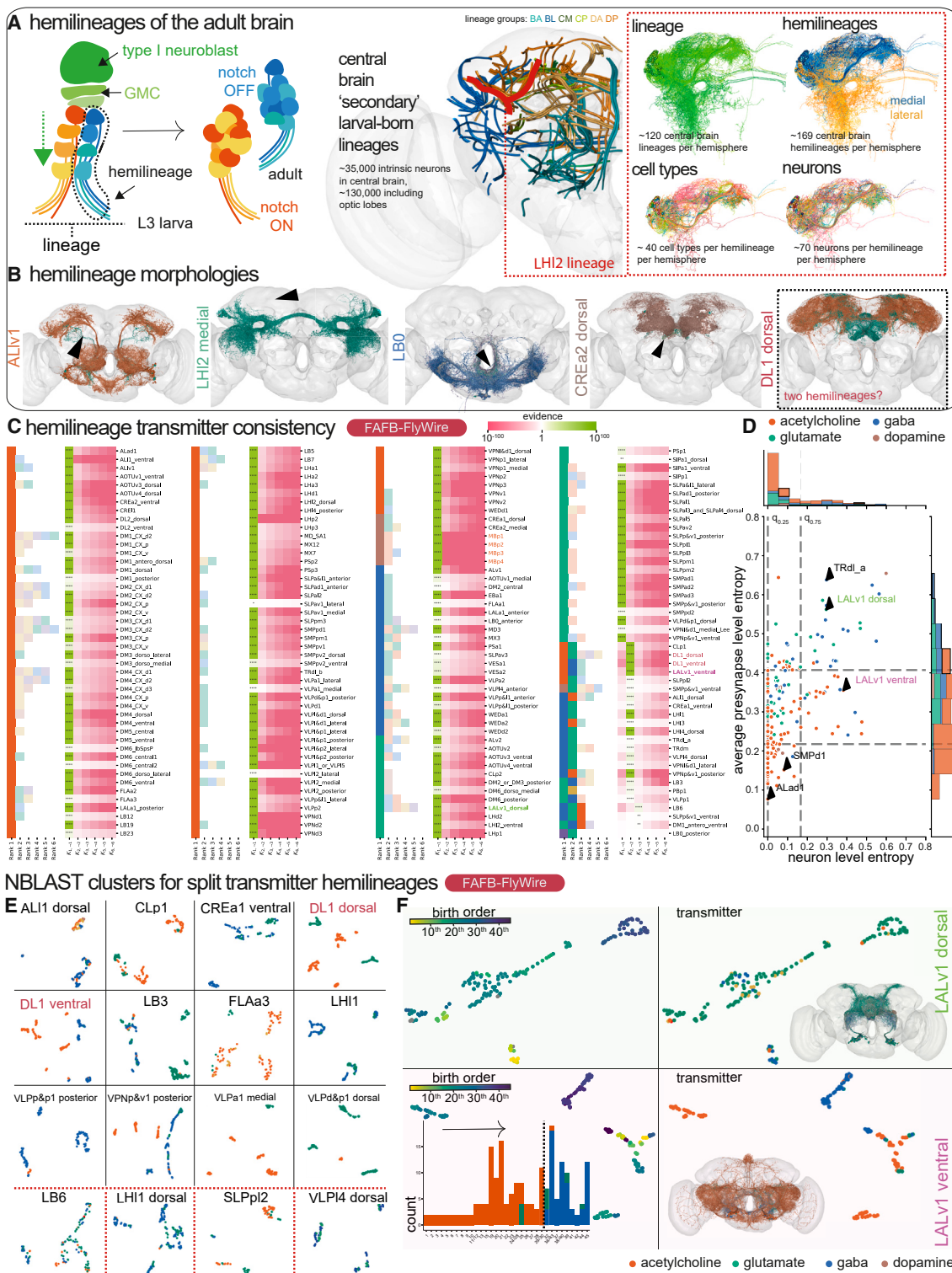


Figure 7. Transmitter usage across all hemilineages in the central fly brain

(A) Left, the progression of a type I neuroblast from third-instar larva (L3) into the adult ganglion mother cell (GMC). Right, a breakdown of a single secondary lineage, "LH12" into its constituent hemilineages (see STAR Methods).

(legend continued on next page)

contralateral turn. If glutamate excited DNao3 (via AMPA, kainate, or NMDA receptors, e.g., Li et al.¹⁰¹) and inhibited MBON26 (e.g., via *GluCl/Alpha*), we might expect unilateral MBON26 activation to result in ipsilateral DNao3 inhibition and contralateral DNao3 activation, and so a stronger contralateral turn command. Therefore, combining both circuit structure and transmitter predictions, we suspect that glutamate both excites and inhibits in this circuit to steer the fly away from an aversive olfactory stimulus.

The distribution of neurotransmitter predictions within developmental units

The nervous system may already naturally group neurons by their transmitter expression because of their development as hemilineages:³¹ these are groups of ~100 neurons that have developed together in a discrete bundle, the hemilineage tract (see STAR Methods for assignment detail). To assess Lacin's law in the brain, we examined the neuron-level transmitter predictions of all neurons in the 183 secondary (larval-born) hemilineages per brain hemisphere in the FlyWire dataset⁵⁰ (Data S5 and Data S6).

We asked how likely it is to observe a given prediction of transmitters in a hemilineage under some error rate given by the confusion matrix on the test set, if Lacin's law is obeyed. We then compared this likelihood to the alternative hypothesis that a hemilineage consists of neurons with more than one transmitter. We calculated the Bayes factor $K_{2,1} = \frac{p(\hat{y}|m=2)}{p(\hat{y}|m=1)}$ and $K_{3,2} = \frac{p(\hat{y}|m=3)}{p(\hat{y}|m=2)}$ for our selected hemilineages from synapse-level transmitter predictions: i.e., the likelihood ratio of the observed model predictions given that a hemilineage expresses two rather than one transmitter or three rather than two transmitters, respectively (see STAR Methods). Maximal one-versus-rest Bayes factors ($K_{m,-m}$) summarized our predictions of the number and set of transmitters for each hemilineage (Figure 7C). We found only 19 of 183 hemilineages with evidence of expressing two transmitters ($n = 19$ decisive) and 3 hemilineages with evidence of expressing three fast-acting transmitters ($n = 1$ decisive, $n = 2$ good). These hemilineages are flagged in Figure 7C.

However, some of these hemilineages (~12) such as "TRdla" and "LALv1 dorsal" showed high synaptic entropy $H(S_h)$ (see STAR Methods, Figure 7D), indicating that individual neurons within the hemilineage contain substantial multimodal transmitter predictions (Figure 7C). As such, multimodality at the neuron level is at least partially explained by uncertain or inhomogeneous predictions between individual synapses within a neuron. This is in contrast to hemilineage "LALv1 ventral," which has a synaptic entropy within the 75% percentile, and for which a large Bayes factor $K_{2,1}$ value directly stems from neuron-level segregation of the predicted transmitters within the hemilineage. We predicted the remaining 163 hemilineages to express a single transmitter ($n = 161$ decisive, $n = 1$ good, $n = 1$ substantial). Results for 154 HemiBrain hemilineages were very similar (Figure S5A, Data S5).

Therefore, 88% of our hemilineages' predictions were strongly biased toward a singular transmitter identity (Figures 7B, 7C, and S5A). The entropy of neuron-level transmitter predictions for each hemilineage was correlated strongly between left and right hemispheres (Figure S5C), suggesting that the observed variation is biological in origin rather than data quality related. In some cases, only a few neurons deviated from the majority prediction (Figure 7B, black arrows). We suspect that these neurons are the "first-born" neurons of the hemilineage, which often have a divergent morphology from the rest of the hemilineage^{31,102}; they may also be divergent in their transmitter usage.

Other prominently split hemilineages also demonstrated morphology-correlated shifts in transmitter expression (Figures 7C, S5A, and S5D). This suggests discrete switches in expression during development, presumably at stereotyped developmental time points. For instance, LALv1 ventral (Figure 7F) revealed a discernible switch in transmitter expression accompanied by morphological differences. Because a recent analysis delineated the birth order of LALv1 neurons,¹⁰² we were able to map this transmission-morphotype switch into its developmental sequence (Figure 7F, lower). In a few cases (Figure 7E, lower), split expression occurred without overt morphological differences, raising questions about sporadic switches and potential confounds. Often, glutamatergic and GABAergic neurons are mixed—our network's most common confusion

(B) Example of homologous FAFB-FlyWire hemilineages on both sides of the brain, colored by neuron-level transmitter prediction. Black arrows point to one stray member of each hemilineage with a different neuron-level transmitter prediction, which is likely a first-born neuron with distinct morphology^{31,102} (Data S5). The dashed box indicates a hemilineage with potential split transmitter expression.

(C) Bayes factor analysis of hemilineage consistency. For each hemilineage (row), the right set of columns corresponds to the likelihood ratio of the hemilineage expressing that number of transmitters versus the likelihood of any other number ($\lambda = 16$; $c_{\text{exp}} = 0.67$). Evidence strength: substantial * $K \geq 10^{1/2}$; good ** $K \geq 10^1$; strong *** $K \geq 10^{3/2}$; decisive **** $K \geq 10^2$.¹⁰³ The left set of columns indicates the frequency ranked transmitter predictions within the hemilineage, with ranks greater than the maximum likely number of transmitters shaded lighter. "LB0 posterior" did not have substantial evidence for any particular number of transmitters.

(D) Neuron level entropy ($H(N_h)$) versus average synapse level entropy ($H(S_h)$) for all predicted hemilineages with more than 10 neurons and more than 30 pre-synapses per neuron. Dashed lines indicate 25% and 75% percentiles: $q_{25}(H(N_h)) = 0.00$, $q_{25}(H(S_h)) = 0.22$, $q_{75}(H(N_h)) = 0.17$, and $q_{75}(H(S_h)) = 0.41$. Type equation here.

(E) NBLAST UMAP plots of selected hemilineages that exhibit some degree of predicted split transmitter usage. UMAPs are based on NBLAST morphological similarity scores between all possible pairs of neurons in each hemilineage. Points represent neurons, colored by neuron-level transmitter prediction. Black solid lines bound examples with a morphology-transmitter split, red dashed lines bound examples with no such clear divide. Red text label examples for which data annotation issues may explain split usage.

(F) "LALv1" has two hemilineages: dorsal (developmentally defined by Notch-ON) and ventral (Notch-OFF). NBLAST UMAPs for the two "LALv1" hemilineages (rows): dorsal (developmentally defined by Notch-ON) and ventral (Notch-OFF), colored by birth order (left) and neuron-level transmitter prediction (right). Bottom left, histogram of neuron-level transmitter prediction by birth order.¹⁰²

See also Figure S5 and Data S6.

(Figure 2A). Notably, potentially as much as 3% of the brain expresses mRNA for machinery related to both,²¹ and at least a few may transmit both.¹⁰⁴ Comparing ~6 GABA-glutamate mixed hemilineages in FlyWire to HemiBrain indicates that perhaps they more uniformly express GABA (Figure S5A). In two cases (the “DL1” hemilineages), we think that the striking morphology-transmitter correlated splits reveal a hemilineage-based division in a lineage-associated tract that was otherwise hard for human annotators to make, i.e., an issue of data annotation.

Challenges surfaced with the “AL1 dorsal” and “ALv2” hemilineages that produce antennal lobe local neurons, a morphologically variable and diverse class of neuron.¹⁰⁵ They seem to break Dale’s law^{104,106} and Lacin’s law (Figure 7C), with similar morphology types predicted to express different transmitters (Figures S5F and S5G). Despite these challenges, we could align our results with existing literature (see STAR Methods). Surprisingly, 18%–27% of antennal lobe local neurons may be cholinergic, suggesting that lateral excitation is a more prominent feature of antennal lobe processing than previously thought.

DISCUSSION

Using high-level annotations to learn low-level features

In evaluating our predictions as broadly as we could, we have found them to be correct for 91% of 624 FAFB-FlyWire cell types and 91% of 524 HemiBrain cell types (Data S7). This result likely depended on three properties of the data that we selected. (1) For both training and inference we used a specific sub-cellular domain (the synapse), likely to contain image features related to our molecules of interest. (2) We aggregated these features on a per-cell basis; this was crucial for linking ground-truth labels and input data and also for improved prediction accuracy. (3) By using cross-modal matching of cell types between EM and light-level neuronal morphology data, we were able to build an expansive ground-truth dataset from molecular information external to the EM data. We anticipate broad applications for this general approach in the biological sciences. Our methodology could be repurposed to identify differences in sub-cellular structures¹⁰⁷ associated with discrete cell types in a range of neuronal and non-neuronal tissues.

Machine learning reveals key molecular descriptors of neuronal function

D. melanogaster represented a hard case for transmitter prediction because humans cannot tell fast-acting transmitters apart in insects. Our classifier accurately predicts transmitter identity from local 3D EM volumes (Figure 2). We find that the overall accuracy of our synapse-level transmitter predictions were slightly more performant in FAFB than in HemiBrain; in particular, HemiBrain is more likely to confuse glutamate for GABA (Figure 2A). This might be because of different sample preparation and staining protocols used for those datasets, our use of only manually annotated presynapses for FAFB ground truth, and/or the higher lateral resolution of FAFB (4 nm vs. 8 nm).

Given that the relationship between synaptic phenotype and transmitter identity is not understood in *D. melanogaster*, we built an explainable AI method that created counterfactual synthetic

images to investigate class differences⁷¹ (Figures 3A and 3B). This enabled us to manually identify at least one feature difference between each pair of fast-acting transmitters (Figure 3C). However, a simple logistic regression classifier trained on three of those features was not able to discriminate between fast-acting transmitters at the same level as the classifier ($n = 219$, 80%/20% randomized training/testing, balanced accuracy 0.52). This indicates that the features we identified are not exhaustive.

We expect our pipeline to be transferable to other connectomic datasets from diverse species. Analogous work detecting excitatory versus inhibitory synapses in the *Ciona intestinalis* larva has added signs for 49 neurons.¹⁰⁸ In vertebrate EM datasets, human annotators can see differences in the vesicles for excitatory and inhibitory synapses.^{16,35–37,109,110} Symmetric synapses (usually inhibitory) have already been disambiguated from asymmetric ones (usually excitatory) automatically and at scale.³⁸ Using our methodology, performant and more specific transmitter predictions are likely to be achievable in both vertebrate and invertebrate datasets.

Sign labeling across a whole-insect central nervous system

Dale’s law, despite its exceptions, serves as a valuable framework for understanding neural action in the face of incomplete data. We needed to use it to accumulate synapse-level transmitter predictions into singular neuron-level transmitter predictions. Extending our conceptual framework, we found that Lacin’s law³¹ is a useful principle that holds in 88% of hemilineages (Figure 7C). We posit that the major exceptions emerge as correlated, discrete switches in both transmitter use and gross morphotype (Figure 7F). Lacin’s law serves the network anatomist in three main ways: supporting prediction validity (Figures S5A and 2D), flagging potential errors when a neuron-level transmitter prediction deviates from the hemilineage majority, and allowing for preliminary transmitter labels to be applied to whole hemilineages in new insect datasets.^{111,112}

The functional role of a synaptic connection depends on upstream transmitters and downstream receptors. Simulating connectomes directly¹¹³ at a whole nervous system scale may be possible with our method (e.g., Shiu et al.¹¹⁴), but incorporating information on postsynaptic receptor expression can make brain models more accurate.¹¹³ Most importantly, while acetylcholine excites and GABA inhibits, glutamate can perform either function in the fly. In the *D. melanogaster* central brain, most reported examples for glutamate are of inhibition via *GluClAlpha* channels.^{89–92,115} The nature of this inhibition could be different, e.g., possibly subtractive⁹¹ rather than divisive.^{86–88,115} Indeed, glutamate may be used more for specific long-range feedforward inhibition and GABA for local divisive inhibition (Figure 6A). However, central excitatory glutamatergic transmission has also been reported.^{93,95,116,117} At the neuromuscular junction, glutamate primarily excites.⁹⁴ We calculated from single-cell RNA sequencing¹¹⁸ that ~80% of neurons in the central brain express RNA transcripts for *GluClAlpha* as well as at least one excitatory ionotropic glutamate receptor. The sign of a glutamatergic connection may depend on the sub-localization and ratio of receptors at recipient sites.¹¹⁹

Beyond fast-acting transmitters, other factors—such as cellular compartments⁸⁰—influence the strengths and signs of neuron-neuron connections. Notably, a large fraction of the synaptic budget is spent on axo-axonic connections (FAFB-FlyWire, 22%; HemiBrain, 20%). Putative inhibitory connections accounted for two-thirds of the axo-axonic sub-budget (Figure 5D) and axons often receive a skewed excitatory:inhibitory connection ratio (Figure 5F). This suggests that the nervous system may employ different circuit logic around axons compared with dendrites.

Limitations of the study

We can think of this study's limitations in two major ways: misprediction (perhaps largely because of co- or alternative transmission, see STAR Methods) by our classifier and other limitations on sign labeling from transmitter identity alone. Outstanding problems that must be solved before we have highly accurate connection signs minimally include: (1) the correction of transmitter mispredictions, (2) the prediction of other transmitters, notably histamine, tyramine, glycine, nitric oxide, and ~53 different neuropeptides, (3) the annotation of monoaminergic co-transmission, (4) the annotation of peptidergic (co-)transmission, (5) the annotation of postsynaptic receptor expression, and (6) the annotation of gap junctions. For (1), community open science annotation projects such as FlyWire via Codex¹²⁰ and Virtual Fly Brain¹²¹ will be valuable. In particular, our least performant predictions were for serotonin. Notably, ~20 known, large, neuropeptidergic neurons are predicted for serotonin. This may be because we included peptidergic, serotonergic neurons in our ground truth.^{122,123} Answers to (2), (3), and (4) could be achieved by linking morphological and transcriptomic cell types⁴⁹ to build more ground truth. One could extend our method to further transmitters and co-transmission combinations as additional training data becomes available (we have shared our literature review of cell type level co-transmission, Data S7). In addition, the detection of individual vesicles, especially dense core vesicles at synapses, or somata could tell us which neurons express neuropeptides and peptide hormones. For problems (5) and (6), linked transcriptomes alone are unlikely either to solve the issue or to provide suitable ground truth for their detection in EM. One path forward would be to assemble ground-truth data with super-resolution light-level microscopy to observe endogenous protein sub-localization^{119,124,125} or with higher-resolution EM to identify key molecules at identified synapses in dense biological samples.¹²⁶ As we showed here with transmitter usage, the identification of some hundreds of pairs of connected neurons may provide sufficient ground truth for a machine-learning solution to predict the remainder across whole nervous systems.

STAR METHODS

Detailed methods are provided in the online version of this paper and include the following:

- KEY RESOURCES TABLE
- RESOURCE AVAILABILITY
 - Lead contact
 - Materials availability

- Data and code availability
- EXPERIMENTAL MODEL AND STUDY PARTICIPANT DETAILS
- METHOD DETAILS
 - Detail on assembling ground truth data for *D. melanogaster*
 - Chosen neuronal reconstructions
 - Neuron skeletonization and axon-dendrite splits
 - Neuron level transmitter prediction confidence
 - Correlating misprediction with reported unlearned transmission types
 - Working through fan-shaped body neuron expression
 - Working through antennal lobe local neuron expression
- HEMILINEAGE DEFINITION IN *D. MELANOGASTER*
 - Hemilineage assignments in *D. melanogaster*
 - Hemilineage prediction entropy
 - Probability to observe transmitter predictions y
 - Bayes Factor
 - Identification of ultrastructural features
 - Advice for resource users
- QUANTIFICATION AND STATISTICAL ANALYSIS

SUPPLEMENTAL INFORMATION

Supplemental information can be found online at <https://doi.org/10.1016/j.cell.2024.03.016>.

ACKNOWLEDGMENTS

This work was supported by a Wellcome Trust Collaborative Award (203261/Z/16/Z), National Institutes of Health (BRAIN Initiative grant 1RF1MH120679-01), an ERC Consolidator grant (649111), and a Neuronex2 award (MC_EX_MR/T046279/1, NSF ref. 2014862), with additional core support from the MRC (MC-U105188491) to G.S.X.E.J.; by the Howard Hughes Medical Institute at Janelia Research Campus (J.F.); and a Boehringer Ingelheim Fonds PhD Fellowship, EMBO fellowship (ALTF 1258-2020), and a Sir Henry Wellcome Postdoctoral Fellowship (222782/Z/21/Z) to A.S.B. Flywire is supported by NIH BRAIN Initiative grant MH117815 to M.M. and S.S. Additional large-scale proofreading and infrastructure was supported by Wellcome awards 203261/Z/16/Z to G.S.X.E.J. and NIH BRAIN Initiative award 1RF1MH120679-01 and NSF NeuroNex award DBI-2014862 to D. Bock and G.S.X.E.J. We thank Laia Serratosa Capdevila (Aelysia Ltd) for copyediting. Please note that we also name individuals from the FAFB community who have assisted with building the data and annotations used in this study in the STAR Methods.

AUTHOR CONTRIBUTIONS

Conceptualization, A.S.B., J.F., and P.S.; methodology A.C., A.S.B., G.S.X.E.J., J.F., M.D., and N.E.; software, A.C., A.S.B., G.S.X.E.J., J.F., M.D., and N.E.; validation, A.C., A.S.B., J.F., M.D., N.E., and P.S.; formal analysis, A.C., A.S.B., J.F., N.E., and Y.Y.; neuroanatomy, A.S.B. and Y.Y.; investigation, A.S.B., J.F., M.D., N.E., and Y.Y.; resources, A.C., A.S.B., G.S.X.E.J., J.F., M.D., N.E., and P.S.; data curation, A.C., A.K.-Y.L., A.S.B., J.F., N.E., P.S., R.P., S.F.-M., T.P., T.R., Y.Y., and V.H.; writing – original draft, A.S.B., G.S.X.E.J., J.F., N.E., and V.H.; writing – review & editing, A.S.B. and J.F.; visualization, A.C., A.S.B., J.F., N.E., and Y.Y.; supervision, A.S.B., G.S.X.E.J., and J.F.; project administration, A.S.B., G.S.X.E.J., and J.F.; funding acquisition, A.S.B., G.S.X.E.J., and J.F. We also credit as authors the key contributors to the FlyWire project, from which we received early data access: FlyWire infrastructure and management, S.D.; FlyWire codex, A.M.; FlyWire proofreader training and community management, A.S., C.M., S.-C.Y., K.E., M.C., and P.S.; FlyWire annotations and cell type matching, P.S., K.E., A.S.B., and G.S.X.E.J.; FlyWire leads, M.M. and S.S.; Cambridge lead, G.S.X.E.J.

DECLARATION OF INTERESTS

The authors declare no competing interests.

Received: April 2, 2023
 Revised: October 4, 2023
 Accepted: March 13, 2024
 Published: May 9, 2024

REFERENCES

1. Cook, S.J., Jarrell, T.A., Brittin, C.A., Wang, Y., Bloniarz, A.E., Yakovlev, M.A., Nguyen, K.C.Q., Tang, L.T.-H., Bayer, E.A., Duerr, J.S., et al. (2019). Whole-animal connectomes of both *caenorhabditis elegans* sexes. *Nature* **571**, 63–71.
2. Ohyama, T., Schneider-Mizell, C.M., Fetter, R.D., Aleman, J.V., Franconville, R., Rivera-Alba, M., Mensh, B.D., Branson, K.M., Simpson, J.H., Truman, J.W., et al. (2015). A multilevel multimodal circuit enhances action selection in *drosophila*. *Nature* **520**, 633–639.
3. Phelps, J.S., Hildebrand, D.G.C., Graham, B.J., Kuan, A.T., Thomas, L.A., Nguyen, T.M., Buhmann, J., Azevedo, A.W., Sustar, A., Agrawal, S., et al. (2021). Reconstruction of motor control circuits in adult *drosophila* using automated transmission electron microscopy. *Cell* **184**, 759–774.e18.
4. Ryan, K., Lu, Z., and Meinertzhagen, I.A. (2016). The cns connectome of a tadpole larva of *ciona intestinalis* (l.) highlights sidedness in the brain of a chordate sibling. *Elife* **5**, e16962.
5. Takemura, S.-Y., Hayworth, K.J., Huang, G.B., Januszewski, M., Lu, Z., Marin, E.C., Preibisch, S., Shan Xu, C., Bogovic, J., Champion, A.S., et al. (2023). A connectome of the male *drosophila* ventral nerve cord. Preprint at bioRxiv. <https://doi.org/10.1101/2023.06.05.543757>.
6. Zheng, Z., Lauritzen, J.S., Perlman, E., Robinson, C.G., Nichols, M., Milkie, D., Torrens, O., Price, J., Fisher, C.B., Sharifi, N., et al. (2018). A complete electron microscopy volume of the brain of adult *drosophila melanogaster*. *Cell* **174**, 730–743.e22.
7. Funke, J., Tschopp, F.D., Grisaitis, W., Sheridan, A., Singh, C., Saalfeld, S., and Turaga, S.C. (2018). Large scale image segmentation with structured loss based deep learning for connectome reconstruction. In *IEEE Transactions on Pattern Analysis and Machine Intelligence*, pp. 1669–1680.
8. Januszewski, M., Kornfeld, J., Li, P.H., Pope, A., Blakely, T., Lindsey, L., Maitin-Shepard, J., Tyka, M., Denk, W., and Jain, V. (2018). High-precision automated reconstruction of neurons with flood-filling networks. *Nat. Methods* **15**, 605–610.
9. Lee, K., Lu, R., Luther, K., and Seung, H.S. (2019). Learning Dense Voxel Embeddings for 3D Neuron Reconstruction. Preprint at arXiv. <https://doi.org/10.48550/arXiv.1909.09872>.
10. Schmidt, M., Motta, A., Sievers, M., and Helmstaedter, M. (2022). RoboEM: automated 3D flight tracing for synaptic-resolution connectomics. Preprint at bioRxiv. <https://doi.org/10.1101/2022.09.08.507122>.
11. Sheridan, A., Nguyen, T.M., Deb, D., Lee, W.-C.A., Saalfeld, S., Turaga, S.C., Manor, U., and Funke, J. (2023). Local shape descriptors for neuron segmentation. *Nat. Methods* **20**, 295–303.
12. Buhmann, J., Sheridan, A., Malin-Mayor, C., Schlegel, P., Gerhard, S., Kazimiers, T., Krause, R., Nguyen, T.M., Heinrich, L., Lee, W.-C.A., et al. (2021). Automatic detection of synaptic partners in a whole-brain *drosophila* electron microscopy data set. *Nat. Methods* **18**, 771–774.
13. Huang, G.B., Scheffer, L.K., and Plaza, S.M. (2018). Fully-Automatic synapse prediction and validation on a large data set. *Front. Neural Circuits* **12**, 87.
14. Kreshuk, A., Funke, J., Cardona, A., and Hamprecht, F.A. (2015). Who is talking to whom: Synaptic partner detection in anisotropic volumes of insect brain. In *Medical Image Computing and Computer-Assisted Intervention – MICCAI 2015*, N. Navab, J. Hornegger, W.M. Wells, and A. Frangi, eds. (Springer International Publishing), pp. 661–668.
15. Staffler, B., Berning, M., Boergens, K.M., Gour, A., Smagt, P.v.d., and Helmstaedter, M. (2017). Synem, automated synapse detection for connectomics. *Elife* **6**, e26414.
16. Svara, F., Förster, D., Kubo, F., Januszewski, M., Dal Maschio, M., Schubert, P.J., Kornfeld, J., Wanner, A.A., Laurell, E., Denk, W., and Baier, H. (2022). Automated synapse-level reconstruction of neural circuits in the larval zebrafish brain. *Nat. Methods* **19**, 1357–1366.
17. Dorkenwald, S., McKellar, C.E., Macrina, T., Kemnitz, N., Lee, K., Lu, R., Wu, J., Popovych, S., Mitchell, E., Nehoran, B., et al. (2022). FlyWire: online community for whole-brain connectomics. *Nat. Methods* **19**, 119–128.
18. Dorkenwald, S., Matsliah, A., Sterling, A.R., Schlegel, P., Yu, S.-C., McKellar, C.E., Lin, A., Costa, M., Eichler, K., Yin, Y., et al. (2023). Neuronal wiring diagram of an adult brain. Preprint at bioRxiv. <https://doi.org/10.1101/2023.06.27.546656>.
19. Winding, M., Pedigo, B.D., Barnes, C.L., Patsolic, H.G., Park, Y., Kazimiers, T., Fushiki, A., Andrade, I.V., Khandelwal, A., Valdes-Aleman, J., et al. (2022). The connectome of an insect brain. *Science* **379**, eadd9330.
20. Azevedo, A., Lesser, E., Mark, B., Phelps, J., Elabbady, L., Kuroda, S., Sustar, A., Moussa, A., Kandelwal, A., Dallmann, C.J., et al. (2022). Tools for comprehensive reconstruction and analysis of *drosophila* motor circuits. Preprint at bioRxiv. <https://doi.org/10.1101/2022.12.15.520299>.
21. Crosset, V., Treiber, C.D., and Waddell, S. (2018). Cellular diversity in the *drosophila* midbrain revealed by single-cell transcriptomics. *Elife* **7**, e34550.
22. Davie, K., Janssens, J., Koldere, D., De Waegeneer, M., Pech, U., Kreft, L., Albar, S., Makhzami, S., Christiaens, V., Bravo González-Blas, C., et al. (2018). A single-cell transcriptome atlas of the aging *drosophila* brain. *Cell* **174**, 982–998.e20.
23. Goyal, R.K., and Chaudhury, A. (2013). Structure activity relationship of synaptic and junctional neurotransmission. *Auton. Neurosci.* **176**, 11–31.
24. Abruzzi, K.C., Zadina, A., Luo, W., Wiyanto, E., Rahman, R., Guo, F., Shaffer, O., and Rosbash, M. (2017). RNA-seq analysis of *drosophila* clock and non-clock neurons reveals neuron-specific cycling and novel candidate neuropeptides. *PLoS Genet.* **13**, e1006613.
25. Aso, Y., Ray, R.P., Long, X., Bushey, D., Cichewicz, K., Ngo, T.-T., Sharp, B., Christoforou, C., Hu, A., Lemire, A.L., et al. (2019). Nitric oxide acts as a cotransmitter in a subset of dopaminergic neurons to diversify memory dynamics. *Elife* **8**, e49257.
26. Yew, J.Y., Wang, Y., Barteneva, N., Dikler, S., Kutz-Naber, K.K., Li, L., and Kravitz, E.A. (2009). Analysis of neuropeptide expression and localization in adult *drosophila melanogaster* central nervous system by affinity cell-capture mass spectrometry. *J. Proteome Res.* **8**, 1271–1284.
27. Nässel, D.R., and Winther, A.M.E. (2010). *Drosophila* neuropeptides in regulation of physiology and behavior. *Prog. Neurobiol.* **92**, 42–104.
28. Taghert, P.H., and Veenstra, J.A. (2003). *Drosophila* neuropeptide signaling. *Adv. Genet.* **49**, 1–65.
29. Nusbaum, M.P., Blitz, D.M., and Marder, E. (2017). Functional consequences of neuropeptide and small-molecule co-transmission. *Nat. Rev. Neurosci.* **18**, 389–403.
30. Deng, B., Li, Q., Liu, X., Cao, Y., Li, B., Qian, Y., Xu, R., Mao, R., Zhou, E., Zhang, W., et al. (2019). Chemoconnectomics: Mapping chemical transmission in *drosophila*. *Neuron* **101**, 876–893.e4.
31. Lacin, H., Chen, H.-M., Long, X., Singer, R.H., Lee, T., and Truman, J.W. (2019). Neurotransmitter identity is acquired in a lineage-restricted manner in the *Drosophila* CNS. *Elife* **8**, e43701.
32. Dale, H. (1935). Pharmacology and nerve endings. *Proc. R. Soc. Med.* **28**, 319–332.
33. Eccles, J.C. (1976). From electrical to chemical transmission in the central nervous system: the closing address of the sir henry dale centennial symposium cambridge, 19 september 1975. *Notes and Records of the Royal Society of London* **30**, 219–230.
34. Yang, C.-P., Fu, C.-C., Sugino, K., Liu, Z., Ren, Q., Liu, L.-Y., Yao, X., Lee, L.P., and Lee, T. (2016). Transcriptomes of lineage-specific *drosophila* neuroblasts profiled by genetic targeting and robotic sorting. *Development* **143**, 411–421.

35. Atwood, H.L., Lang, F., and Morin, W.A. (1972). Synaptic vesicles: selective depletion in crayfish excitatory and inhibitory axons. *Science* **176**, 1353–1355.
36. Tao, C.-L., Liu, Y.-T., Sun, R., Zhang, B., Qi, L., Shivakoti, S., Tian, C.-L., Zhang, P., Lau, P.-M., Zhou, Z.H., and Bi, G.-Q. (2018). Differentiation and characterization of excitatory and inhibitory synapses by cryo-electron tomography and correlative microscopy. *J. Neurosci.* **38**, 1493–1510.
37. Uchizono, K. (1965). Characteristics of excitatory and inhibitory synapses in the central nervous system of the cat. *Nature* **207**, 642–643.
38. Dorkenwald, S., Schubert, P.J., Killinger, M.F., Urban, G., Mikula, S., Svara, F., and Kornfeld, J. (2017). Automated synaptic connectivity inference for volume electron microscopy. *Nat. Methods* **14**, 435–442.
39. Davis, F.P., Nern, A., Picard, S., Reiser, M.B., Rubin, G.M., Eddy, S.R., and Henry, G.L. (2020). A genetic, genomic, and computational resource for exploring neural circuit function. *Elife* **9**, e50901.
40. Henry, G.L., Davis, F.P., Picard, S., and Eddy, S.R. (2012). Cell type-specific genomics of drosophila neurons. *Nucleic Acids Res.* **40**, 9691–9704.
41. Hyatt, A.D., and Wise, T.G. (2001). Immunolabeling. In *Immunocytochemistry and In Situ Hybridization in the Biomedical Sciences* (Springer), pp. 73–107.
42. Konstantinides, N., Rossi, A.M., and Desplan, C. (2015). Common temporal identity factors regulate neuronal diversity in fly ventral nerve cord and mouse retina. *Neuron* **85**, 447–449.
43. Long, X., Colonell, J., Wong, A.M., Singer, R.H., and Lionnet, T. (2017). Quantitative mrna imaging throughout the entire drosophila brain. *Nat. Methods* **14**, 703–706.
44. Meissner, G.W., Nern, A., Singer, R.H., Wong, A.M., Malkesman, O., and Long, X. (2019). Mapping neurotransmitter identity in the whole-mount drosophila brain using multiplex high-throughput fluorescence *in situ* hybridization. *Genetics* **211**, 473–482.
45. Jenett, A., Rubin, G.M., Ngo, T.T.B., Shepherd, D., Murphy, C., Dionne, H., Pfeiffer, B.D., Cavallaro, A., Hall, D., Jeter, J., et al. (2012). A GAL4-Driver line resource for drosophila neurobiology. *Cell Rep.* **2**, 991–1001.
46. Luan, H., Diao, F., Scott, R.L., and White, B.H. (2020). The drosophila split gal4 system for neural circuit mapping. *Front. Neural Circuits* **14**, 603397.
47. Costa, M., Manton, J.D., Ostrovsky, A.D., Prohaska, S., and Jefferis, G.S.X.E. (2016). NBLAST: Rapid, sensitive comparison of neuronal structure and construction of neuron family databases. *Neuron* **91**, 293–311.
48. Otsuna, H., Ito, M., and Kawase, T. (2018). Color depth MIP mask search: a new tool to expedite Split-GAL4 creation. Preprint at bioRxiv. <https://doi.org/10.1101/318006>.
49. Bates, A.S., Janssens, J., Jefferis, G.S., and Aerts, S. (2019). Neuronal cell types in the fly: single-cell anatomy meets single-cell genomics. *Curr. Opin. Neurobiol.* **56**, 125–134.
50. Schlegel, P., Yin, Y., Bates, A.S., Dorkenwald, S., Eichler, K., Brooks, P., Han, D.S., Gkantia, M., dos Santos, M., Munnelly, E.J., et al. (2023). A consensus cell type atlas from multiple connectomes reveals principles of circuit stereotypy and variation. Preprint at bioRxiv. <https://doi.org/10.1101/2023.06.27.546055>.
51. Scheffer, L.K., Xu, C.S., Januszewski, M., Lu, Z., Takemura, S.-Y., Hayworth, K.J., Huang, G.B., Shinomiya, K., Maitlin-Shepard, J., Berg, S., et al. (2020). A connectome and analysis of the adult drosophila central brain. *Elife* **9**, e57443.
52. Simonyan, K., and Zisserman, A. (2014). Very deep convolutional networks for large-scale image recognition. Preprint at arXiv. <https://doi.org/10.48550/arXiv.1409.1556>.
53. Kingma, D.P., and Ba, J. (2014). Adam: A method for stochastic optimization. Preprint at arXiv. <https://doi.org/10.48550/arXiv.1412.6980>.
54. Ito, K., Shinomiya, K., Ito, M., Armstrong, J.D., Boyan, G., Hartenstein, V., Harzsch, S., Heisenberg, M., Homberg, U., Jenett, A., et al. (2014). A systematic nomenclature for the insect brain. *Neuron* **81**, 755–765.
55. Barnstedt, O., Owald, D., Felsenberg, J., Brain, R., Moszynski, J.-P., Talbot, C.B., Perrat, P.N., and Waddell, S. (2016). Memory-Relevant mushroom body output synapses are cholinergic. *Neuron* **89**, 1237–1247.
56. Haynes, P.R., Christmann, B.L., and Griffith, L.C. (2015). A single pair of neurons links sleep to memory consolidation in *drosophila melanogaster*. *Elife* **4**, e03868.
57. Omoto, J.J., Nguyen, B.-C.M., Kandimalla, P., Lovick, J.K., Donlea, J.M., and Hartenstein, V. (2018). Putative interactions within the drosophila ellipsoid body neuropil. *Front. Neural Circuits* **12**, 103.
58. Park, S.K., George, R., Cai, Y., Chang, H.Y., Krantz, D.E., Friggi-Grelin, F., Birman, S., and Hirsh, J. (2006). Cell-type-specific limitation on *in vivo* serotonin storage following ectopic expression of the drosophila serotonin transporter, dSERT. *J. Neurobiol.* **66**, 452–462.
59. Shih, H.-W., and Chiang, A.-S. (2011). Anatomical characterization of thermosensory AC neurons in the adult drosophila brain. *J. Neurogenet.* **25**, 1–6.
60. Waddell, S., Armstrong, J.D., Kitamoto, T., Kaiser, K., and Quinn, W.G. (2000). The amnesiac gene product is expressed in two neurons in the drosophila brain that are critical for memory. *Cell* **103**, 805–813.
61. Das, A., Chiang, A., Davla, S., Priya, R., Reichert, H., VijayRaghavan, K., and Rodrigues, V. (2011a). Identification and analysis of a glutamatergic local interneuron lineage in the adult drosophila olfactory system. *Neural Syst. Circuits* **1**, 4.
62. Python, F., and Stocker, R.F. (2002). Immunoreactivity against choline acetyltransferase, gamma-aminobutyric acid, histamine, octopamine, and serotonin in the larval chemosensory system of dosophila melanogaster. *J. Comp. Neurol.* **453**, 157–167.
63. Shang, Y., Claridge-Chang, A., Sjulson, L., Pypaert, M., and Miesenböck, G. (2007). Excitatory local circuits and their implications for olfactory processing in the fly antennal lobe. *Cell* **128**, 601–612.
64. Yasuyama, K., and Salvaterra, P.M. (1999). Localization of choline acetyltransferase-expressing neurons in drosophila nervous system. *Microsc. Res. Tech.* **45**, 65–79.
65. Marin, E.C., Morris, B.J., Stuerner, T., Champion, A.S., Krzeminski, D., Badalamente, G., Gkantia, M., Dunne, C.R., Eichler, K., Takemura, S.-Y., et al. (2023). Systematic annotation of a complete adult male drosophila nerve cord connectome reveals principles of functional organisation. Preprint at bioRxiv. <https://doi.org/10.1101/2023.06.05.543407>.
66. Ancona, M., Ceolini, E., Öztireli, C., and Gross, M. (2018). Towards better understanding of gradient-based attribution methods for deep neural networks. In *International Conference on Learning Representations*.
67. Selvaraju, R.R., Cogswell, M., Das, A., Vedantam, R., Parikh, D., and Batra, D. (2017). Grad-cam: Visual explanations from deep networks via gradient-based localization. In *Proceedings of the IEEE international conference on computer vision*, pp. 618–626.
68. Shrikumar, A., Greenside, P., Shcherbina, A., and Kundaje, A. (2016). Not just a black box: Learning important features through propagating activation differences. Preprint at arXiv. <https://doi.org/10.48550/arXiv.1605.01713>.
69. Sundararajan, M., Taly, A., and Yan, Q. (2017). Axiomatic attribution for deep networks. In *Proceedings of the 34th International Conference on Machine Learning, Volume 70 (JMLR.org)*, pp. 3319–3328.
70. Kindermans, P.-J., Schütt, K.T., Alber, M., Müller, K.-R., Erhan, D., Kim, B., and Dähne, S. (2017). Learning how to explain neural networks: Patternnet and patternattribution. Preprint at arXiv. <https://doi.org/10.48550/arXiv.1705.05598>.
71. Eckstein, N., Bukhari, H., Bates, A.S., Jefferis, G.S., and Funke, J. (2023). Discriminative attribution from paired images. In *Computer Vision-ECCV 2022 Workshops: Tel Aviv, Israel, October 23–27, 2022, Proceedings, Part IV (Springer)*, pp. 406–422.

72. Zhu, J.-Y., Park, T., Isola, P., and Efros, A.A. (2017). Unpaired image-to-image translation using cycle-consistent adversarial networks. In Proceedings of the IEEE international conference on computer vision, pp. 2223–2232.
73. Schneider-Mizell, C.M., Gerhard, S., Longair, M., Kazimiers, T., Li, F., Zwart, M.F., Champion, A., Midgley, F.M., Fetter, R.D., Saalfeld, S., and Cardona, A. (2016). Quantitative neuroanatomy for connectomics in *drosophila*. *Elife* 5, e12059.
74. Schlegel, P., Bates, A.S., Stürner, T., Jagannathan, S.R., Drummond, N., Hsu, J., Serratosa Capdevila, L., Javier, A., Marin, E.C., Barth-Maron, A., et al. (2021). Information flow, cell types and stereotypy in a full olfactory connectome. *Elife* 10, e66018.
75. Pires, P.M., Abbott, L.F., and Maimon, G. (2024). Converting an allocentric goal into an egocentric steering signal. *Nature* 626, 808–818.
76. Westeinde, E.A., Kellogg, E., Dawson, P.M., Lu, J., Hamburg, L., Midler, B., Druckmann, S., and Wilson, R.I. (2024). Transforming a head direction signal into a goal-oriented steering command. *Nature* 626, 819–826.
77. Hulse, B.K., Haberkern, H., Franconville, R., Turner-Evans, D., Take-mura, S.-Y., Wolff, T., Noorman, M., Dreher, M., Dan, C., Parekh, R., et al. (2021). A connectome of the *drosophila* central complex reveals network motifs suitable for flexible navigation and context-dependent action selection. *Elife* 10, e66039.
78. Mao, Z., and Davis, R.L. (2009). Eight different types of dopaminergic neurons innervate the *drosophila* mushroom body neuropil: anatomical and physiological heterogeneity. *Front. Neural Circuits* 3, 5.
79. Aso, Y., Hattori, D., Yu, Y., Johnston, R.M., Iyer, N.A., Ngo, T.T.B., Dionne, H., Abbott, L.F., Axel, R., Tanimoto, H., and Rubin, G.M. (2014). The neuronal architecture of the mushroom body provides a logic for associative learning. *Elife* 3, e04577.
80. Liu, T.X., Davoudian, P.A., Lizbinski, K.M., and Jeanne, J.M. (2022). Connectomic features underlying diverse synaptic connection strengths and subcellular computation. *Curr. Biol.* 32, 559–569.e5.
81. Ramon Cajal, S. (1911). Histologie du système nerveux de l'homme et des vertébrés. grand sympathique2 (Paris Maloine), pp. 891–942.
82. Dolan, M.-J., Belliart-Guérin, G., Bates, A.S., Frechter, S., Lampin-Saint-Amaux, A., Aso, Y., Roberts, R.J.V., Schlegel, P., Wong, A., Hammad, A., et al. (2018). Communication from learned to innate olfactory processing centers is required for memory retrieval in *Drosophila*. *Neuron* 100, 651–668.
83. Rolls, M.M. (2011). Neuronal polarity in *drosophila*: sorting out axons and dendrites. *Dev. Neurobiol.* 71, 419–429.
84. Bossy, B., Ballivet, M., and Spierer, P. (1988). Conservation of neural nicotinic acetylcholine receptors from *drosophila* to vertebrate central nervous systems. *EMBO J.* 7, 611–618.
85. Schuster, R., Phannavong, B., Schröder, C., and Gundelfinger, E.D. (1993). Immunohistochemical localization of a ligand-binding and a structural subunit of nicotinic acetylcholine receptors in the central nervous system of *drosophila melanogaster*. *J. Comp. Neurol.* 335, 149–162.
86. Olsen, S.R., Bhandawat, V., and Wilson, R.I. (2010). Divisive normalization in olfactory population codes. *Neuron* 66, 287–299.
87. Olsen, S.R., and Wilson, R.I. (2008). Lateral presynaptic inhibition mediates gain control in an olfactory circuit. *Nature* 452, 956–960.
88. Wilson, R.I., and Laurent, G. (2005). Role of GABAergic inhibition in shaping odor-evoked spatiotemporal patterns in the *Drosophila* antennal lobe. *J. Neurosci.* 25, 9069–9079.
89. Liu, W.W., and Wilson, R.I. (2013). Glutamate is an inhibitory neurotransmitter in the *Drosophila* olfactory system. *Proc. Natl. Acad. Sci. USA* 110, 10294–10299.
90. Lu, J., Behbahani, A.H., Hamburg, L., Westeinde, E.A., Dawson, P.M., Lyu, C., Maimon, G., Dickinson, M.H., Druckmann, S., and Wilson, R.I. (2022). Transforming representations of movement from body- to world-centric space. *Nature* 601, 98–104.
91. McCarthy, E.V., Wu, Y., Decarvalho, T., Brandt, C., Cao, G., and Nitabach, M.N. (2011). Synchronized bilateral synaptic inputs to *drosophila melanogaster* neuropeptidergic rest/arousal neurons. *J. Neurosci.* 31, 8181–8193.
92. Molina-Obando, S., Vargas-Fique, J.F., Henning, M., Gür, B., Schladt, T.M., Akhtar, J., Berger, T.K., and Silies, M. (2019). ON selectivity in the *drosophila* visual system is a multisynaptic process involving both glutamatergic and GABAergic inhibition. *Elife* 8, e49373.
93. Ichinose, T., Aso, Y., Yamagata, N., Abe, A., Rubin, G.M., and Tanimoto, H. (2015). Reward signal in a recurrent circuit drives appetitive long-term memory formation. *Elife* 4, e10719.
94. Jan, L.Y., and Jan, Y.N. (1976). L-glutamate as an excitatory transmitter at the *drosophila* larval neuromuscular junction. *J. Physiol.* 262, 215–236.
95. Zhao, X., Lenek, D., Dag, U., Dickson, B.J., and Keleman, K. (2018). Persistent activity in a recurrent circuit underlies courtship memory in *drosophila*. *Elife* 7.
96. Felsenberg, J., Jacob, P.F., Walker, T., Barnstedt, O., Edmondson-Stait, A.J., Pleijzier, M.W., Otto, N., Schlegel, P., Sharifi, N., Perisse, E., et al. (2018). Integration of parallel opposing memories underlies memory extinction. *Cell* 175, 709–722.e15.
97. Bates, A.S., Schlegel, P., Roberts, R.J.V., Drummond, N., Tamimi, I.F.M., Turnbull, R., Zhao, X., Marin, E.C., Popovici, P.D., Dhawan, S., et al. (2020b). Complete connectomic reconstruction of olfactory projection neurons in the fly brain. *Curr. Biol.* 30, 3183–3199.e6.
98. Wilson, R.I., and Mainen, Z.F. (2006). Early events in olfactory processing. *Annu. Rev. Neurosci.* 29, 163–201.
99. Cheong, H.S.J., Eichler, K., Stuerner, T., Asinof, S.K., Champion, A.S., Marin, E.C., Oram, T.B., Sumathipala, M., Venkatasubramanian, L., Namiki, S., et al. (2023). Transforming descending input into behavior: The organization of premotor circuits in the *drosophila* male adult nerve cord connectome. Preprint at bioRxiv. <https://doi.org/10.1101/2023.06.07.543976>.
100. Rubin, G.M., and Aso, Y. (2023). New genetic tools for mushroom body output neurons in *drosophila*.
101. Li, Y., Dharkar, P., Han, T.-H., Serpe, M., Lee, C.-H., and Mayer, M.L. (2016). Novel functional properties of *drosophila* CNS glutamate receptors. *Neuron* 92, 1036–1048.
102. Lee, Y.-J., Yang, C.-P., Miyares, R.L., Huang, Y.-F., He, Y., Ren, Q., Chen, H.-M., Kawase, T., Ito, M., Otsuna, H., et al. (2020). Conservation and divergence of related neuronal lineages in the *drosophila* central brain. *Elife* 9, e53518.
103. Jeffreys, H. (1998). The theory of probability (OUP Oxford).
104. Das, S., Sadanandappa, M.K., Dervan, A., Larkin, A., Lee, J.A., Sudhakaran, I.P., Priya, R., Heidari, R., Holohan, E.E., Pimentel, A., et al. (2011b). Plasticity of local GABAergic interneurons drives olfactory habituation. *Proc. Natl. Acad. Sci. USA* 108, E646–E654.
105. Chou, Y.-H., Spletter, M.L., Yaksi, E., Leong, J.C.S., Wilson, R.I., and Luo, L. (2010). Diversity and wiring variability of olfactory local interneurons in the *drosophila* antennal lobe. *Nat. Neurosci.* 13, 439–449.
106. Carlsson, M.A., Diesner, M., Schachtner, J., and Nässel, D.R. (2010). Multiple neuropeptides in the *drosophila* antennal lobe suggest complex modulatory circuits. *J. Comp. Neurol.* 518, 3359–3380.
107. Xu, C.S., Pang, S., Shtengel, G., Müller, A., Ritter, A.T., Hoffman, H.K., Take-mura, S.-Y., Lu, Z., Pasolli, H.A., Iyer, N., et al. (2021). An open-access volume electron microscopy atlas of whole cells and tissues. *Nature* 599, 147–151.
108. Zhang, A., Shailja, S., Borba, C., Miao, Y., Goebel, M., Ruschel, R., Ryan, K., Smith, W., and Manjunath, B.S. (2022). Automatic classification and neurotransmitter prediction of synapses in electron microscopy. *Biol. Imaging* 2, e6.
109. Colonnier, M. (1968). Synaptic patterns on different cell types in the different laminae of the cat visual cortex. an electron microscope study. *Brain Res.* 9, 268–287.

110. Gray, E.G. (1959). Axo-somatic and axo-dendritic synapses of the cerebral cortex: an electron microscope study. *J. Anat.* 93 (Pt 4), 420–433.
111. Siegler, M.V., Pankhaniya, R.R., and Jia, X.X. (2001). Pattern of expression of engrailed in relation to gamma-aminobutyric acid immunoreactivity in the central nervous system of the adult grasshopper. *J. Comp. Neurol.* 440, 85–96.
112. Witten, J.L., and Truman, J.W. (1998). Distribution of GABA-like immunoreactive neurons in insects suggests lineage homology. *J. Comp. Neurol.* 398, 515–528.
113. Lappalainen, J.K., Tschopp, F.D., Prakhy, S., McGill, M., Nern, A., Shinomiya, K., Takemura, S.-y., Gruntman, E., Macke, J.H., and Turaga, S.C. (2023). Connectome-constrained deep mechanistic networks predict neural responses across the fly visual system at single-neuron resolution. Preprint at bioRxiv. <https://doi.org/10.1101/2023.03.11.532232>.
114. Shiu, P.K., Sterne, G.R., Spiller, N., Franconville, R., Sandoval, A., Zhou, J., Simha, N., Kang, C.H., Yu, S., Kim, J.S., et al. (2023). A leaky integrate-and-fire computational model based on the connectome of the entire adult drosophila brain reveals insights into sensorimotor processing. Preprint at bioRxiv. <https://doi.org/10.1101/2023.05.02.539144>.
115. Groschner, L.N., Malis, J.G., Zuidinga, B., and Borst, A. (2022). A biophysical account of multiplication by a single neuron. *Nature* 603, 119–123.
116. Miyashita, T., Murakami, K., Kikuchi, E., Ofusa, K., Mikami, K., Endo, K., Miyaji, T., Moriyama, S., Konno, K., Muratani, H., et al. (2023). Glia transmit negative valence information during aversive learning in *Drosophila*. *Science* 382, eadf7429.
117. Ni, J.D., Gurav, A.S., Liu, W., Ogunmowo, T.H., Hackbart, H., Elsheikh, A., Verdegaaal, A.A., and Montell, C. (2019). Differential regulation of the drosophila sleep homeostat by circadian and arousal inputs. *Elife* 8, e40487.
118. Park, A., Croset, V., Otto, N., Agarwal, D., Treiber, C.D., Meschi, E., Sims, D., and Waddell, S. (2022). Gliotransmission of d-serine promotes thirst-directed behaviors in drosophila. *Curr. Biol.* 32, 3952–3970.e8.
119. Sanfilippo, P., Kim, A.J., Bhukel, A., Yoo, J., Mirshahidi, P.S., Pandey, V., Bevir, H., Yuen, A., Mirshahidi, P.S., Guo, P., et al. (2023). Mapping of multiple neurotransmitter receptor subtypes and distinct protein complexes to the connectome. Preprint at bioRxiv. <https://doi.org/10.1101/2023.10.02.560011>.
120. Dorkenwald, S., Schneider-Mizell, C.M., Brittain, D., Halageri, A., Jordan, C., Kemnitz, N., Castro, M.A., Silversmith, W., Maitin-Shephard, J., Troidl, J., et al. (2023). CAVE: Connectome annotation versioning engine. Preprint at bioRxiv. <https://doi.org/10.1101/2023.07.26.550598>.
121. Court, R., Costa, M., Pilgrim, C., Millburn, G., Holmes, A., McLachlan, A., Larkin, A., Matentzoglu, N., Kir, H., Parkinson, H., et al. (2023). Virtual fly Brain-An interactive atlas of the drosophila nervous system. *Front. Physiol.* 14, 1076533.
122. Jiang, H., Lkhagva, A., Daubnerová, I., Chae, H.-S., Šimo, L., Jung, S.-H., Yoon, Y.-K., Lee, N.-R., Seong, J.Y., Žitňan, D., et al. (2013). Natalisin, a tachykinin-like signaling system, regulates sexual activity and fecundity in insects. *Proc. Natl. Acad. Sci. USA* 110, E3526–E3534.
123. Scheunemann, L., Plaçais, P.Y., Dromard, Y., Schwärzel, M., and Preat, T. (2018). Dunce phosphodiesterase acts as a checkpoint for drosophila Long-Term memory in a pair of serotonergic neurons. *Neuron* 98, 350–365.e5.
124. Kondo, S., Takahashi, T., Yamagata, N., Imanishi, Y., Katow, H., Hiramatsu, S., Lynn, K., Abe, A., Kumaraswamy, A., and Tanimoto, H. (2020). Neurochemical organization of the drosophila brain visualized by endogenously tagged neurotransmitter receptors. *Cell Rep.* 30, 284–297.e5.
125. Lillvis, J.L., Otsuna, H., Ding, X., Pisarev, I., Kawase, T., Colonell, J., Rokicki, K., Goina, C., Gao, R., Hu, A., et al. (2022). Rapid reconstruction of neural circuits using tissue expansion and light sheet microscopy. *Elife* 11, e81248.
126. Rickgauer, J.P., Grigorieff, N., and Denk, W. (2017). Single-protein detection in crowded molecular environments in cryo-EM images. *Elife* 6, e25648.
127. Matheson, A.M.M., Lanz, A.J., Medina, A.M., Licata, A.M., Currier, T.A., Syed, M.H., and Nagel, K.I. (2022). A neural circuit for wind-guided olfactory navigation. *Nat. Commun.* 13, 4613.
128. Schlegel, P., Gokaslan, A., and Kazimiers, T. (2022). navis-org/skeletor: Version 1.2.3.
129. Sayin, S., De Backer, J.-F., Siju, K.P., Wosniack, M.E., Lewis, L.P., Frisch, L.-M., Gansen, B., Schlegel, P., Edmondson-Stait, A., Sharifi, N., et al. (2019). A neural circuit arbitrates between persistence and withdrawal in hungry *Drosophila*. *Neuron* 104, 544–558.e6.
130. R Core Team (2021). R: A Language and Environment for Statistical Computing (R Foundation for Statistical Computing).
131. Xie, Y. (2015). Dynamic Documents with R and knitr (Chapman and Hall).
132. Wickham, H. (2011). Ggplot2. *WIREs Computational Stats.* 3, 180–185.
133. Bates, A.S., Manton, J.D., Jagannathan, S.R., Costa, M., Schlegel, P., Rohlfing, T., and Jefferis, G.S. (2020a). The natverse, a versatile toolbox for combining and analysing neuroanatomical data. *Elife* 9, e53350.
134. Veveryta, L., and Allan, D.W. (2013). Subtype-specific neuronal remodeling during *Drosophila* metamorphosis. *Fly* 7, 78–86.
135. Plaza, S.M., Clements, J., Dolafi, T., Umayam, L., Neubarth, N.N., Scheffer, L.K., and Berg, S. (2022). neuprint: An open access tool for EM connectomics. *Front. Neuroinform.* 16, 896292.
136. Knott, G., Marchman, H., Wall, D., and Lich, B. (2008). Serial section scanning electron microscopy of adult brain tissue using focused ion beam milling. *J. Neurosci.* 28, 2959–2964.
137. Li, P.H., Lindsey, L.F., Januszewski, M., Zheng, Z., Bates, A.S., Taisz, I., Tyka, M., Nichols, M., Li, F., Perlman, E., et al. (2020b). Automated reconstruction of a Serial-Section EM drosophila brain with Flood-Filling networks and local realignment. Preprint at bioRxiv. <https://doi.org/10.1101/605634>.
138. Busch, S., Selcho, M., Ito, K., and Tanimoto, H. (2009). A map of octopaminergic neurons in the *Drosophila* brain. *J. Comp. Neurol.* 513, 643–667.
139. Ito, M., Masuda, N., Shinomiya, K., Endo, K., and Ito, K. (2013). Systematic analysis of neural projections reveals clonal composition of the *Drosophila* brain. *Curr. Biol.* 23, 644–655.
140. Bräcker, L.B., Siju, K.P., Varela, N., Aso, Y., Zhang, M., Hein, I., Vasconcelos, M.L., and Grunwald Kadow, I.C. (2013). Essential role of the mushroom body in context-dependent CO₂ avoidance in *Drosophila*. *Curr. Biol.* 23, 1228–1234.
141. Dacks, A.M., Christensen, T.A., and Hildebrand, J.G. (2006). Phylogeny of a serotonin-immunoreactive neuron in the primary olfactory center of the insect brain. *J. Comp. Neurol.* 498, 727–746.
142. Dolan, M.-J., Frechter, S., Bates, A.S., Dan, C., Huoviala, P., Roberts, R.J., Schlegel, P., Dhawan, S., Tabano, R., Dionne, H., et al. (2019). Neurogenetic dissection of the drosophila lateral horn reveals major outputs, diverse behavioural functions, and interactions with the mushroom body. *Elife* 8, e43079.
143. Frenkel, L., Muraro, N.I., Beltrán González, A.N., Marcora, M.S., Berribó, G., Hermann-Luibl, C., Romero, J.I., Helfrich-Förster, C., Castaño, E.M., Marino-Busjle, C., et al. (2017). Organization of circadian behavior relies on glycinergic transmission. *Cell Rep.* 19, 72–85.
144. Guo, F., Yu, J., Jung, H.J., Abruzzi, K.C., Luo, W., Griffith, L.C., and Rosbash, M. (2016). Circadian neuron feedback controls the drosophila sleep–activity profile. *Nature* 536, 292–297.
145. Krashes, M.J., DasGupta, S., Vreede, A., White, B., Armstrong, J.D., and Waddell, S. (2009). A neural circuit mechanism integrating motivational state with memory expression in drosophila. *Cell* 139, 416–427.
146. Lai, S.-L., Awasaki, T., Ito, K., and Lee, T. (2008). Clonal analysis of *Drosophila* antennal lobe neurons: diverse neuronal architectures in the lateral neuroblast lineage. *Development* 135, 2883–2893.

147. Liu, C., Meng, Z., Wiggin, T.D., Yu, J., Reed, M.L., Guo, F., Zhang, Y., Rosbash, M., and Griffith, L.C. (2019). A Serotonin-Modulated circuit controls sleep architecture to regulate cognitive function independent of total sleep in *drosophila*. *Curr. Biol.* **29**, 3635–3646.e5.
148. Liu, X., Buchanan, M.E., Han, K.-A., and Davis, R.L. (2009). The GABA receptor RDL suppresses the conditioned stimulus pathway for olfactory learning. *J. Neurosci.* **29**, 1573–1579.
149. Nässel, D.R., and Elekes, K. (1992). Aminergic neurons in the brain of blowflies and *drosophila*: dopamine- and tyrosine hydroxylase-immuno-reactive neurons and their relationship with putative histaminergic neurons. *Cell Tissue Res.* **267**, 147–167.
150. Niens, J., Reh, F., Çoban, B., Cichewicz, K., Eckardt, J., Liu, Y.-T., Hirsh, J., and Riemensperger, T.D. (2017). Dopamine modulates serotonin innervation in the *drosophila* brain. *Front. Syst. Neurosci.* **11**, 76.
151. Okada, R., Awasaki, T., and Ito, K. (2009). Gamma-aminobutyric acid (GABA)-mediated neural connections in the *Drosophila* antennal lobe. *J. Comp. Neurol.* **514**, 74–91.
152. Palavicino-Maggio, C.B., Chan, Y.-B., McKellar, C., and Kravitz, E.A. (2019). A small number of cholinergic neurons mediate hyperaggression in female *Drosophila*. *Proc. Natl. Acad. Sci. USA* **116**, 17029–17038.
153. Senapati, B., Tsao, C.-H., Juan, Y.-A., Chiu, T.-H., Wu, C.-L., Waddell, S., and Lin, S. (2019). A neural mechanism for deprivation state-specific expression of relevant memories in *drosophila*. *Nat. Neurosci.* **22**, 2029–2039.
154. Shafer, O.T., Helfrich-Förster, C., Renn, S.C.P., and Taghert, P.H. (2006). Reevaluation of *drosophila melanogaster*'s neuronal circadian pacemakers reveals new neuronal classes. *J. Comp. Neurol.* **498**, 180–193.
155. Shinomiya, K., Takemura, S.-Y., Rivlin, P.K., Plaza, S.M., Scheffer, L.K., and Meinertzhagen, I.A. (2015). A common evolutionary origin for the ON- and OFF-edge motion detection pathways of the *Drosophila* visual system. *Front. Neural Circuits* **9**, 33.
156. Tanaka, N.K., Endo, K., and Ito, K. (2012). Organization of antennal lobe-associated neurons in adult *Drosophila melanogaster* brain. *J. Comp. Neurol.* **520**, 4067–4130.
157. Turner-Evans, D.B., Jensen, K.T., Ali, S., Paterson, T., Sheridan, A., Ray, R.P., Wolff, T., Lauritzen, J.S., Rubin, G.M., Bock, D.D., and Jayaraman, V. (2020). The neuroanatomical ultrastructure and function of a biological ring attractor. *Neuron* **108**, 145–163.e10.
158. Wolff, T., Iyer, N.A., and Rubin, G.M. (2015). Neuroarchitecture and neuroanatomy of the *drosophila* central complex: A GAL4-based dissection of protocerebral bridge neurons and circuits. *J. Comp. Neurol.* **523**, 997–1037.
159. Frechter, S., Bates, A.S., Tootoonian, S., Dolan, M.-J., Manton, J.D., Jamasb, A.R., Kohl, J., Bock, D., and Jefferis, G.S. (2019). Functional and anatomical specificity in a higher olfactory centre. *Elife* **8**, e44590.
160. Huoviala, P., Dolan, M.-J., Love, F.M., Frechter, S., Roberts, R.J.V., Mirevica, Z., Schlegel, P., Bates, A.S., Aso, Y., Rodrigues, T., et al. (2018). Neural circuit basis of aversive odour processing in *Drosophila* from sensory input to descending output. Preprint at bioRxiv. <https://doi.org/10.1101/394403>.
161. Marin, E.C., Roberts, R.J.V., Büld, L., Theiss, M., Pleijzier, M.W., Sarkisian, T., Laursen, W.J., Turnbull, R., Schlegel, P., Bates, A.S., et al. (2020). Connectomics analysis reveals first, second, and third order thermosensory and hygrosensory neurons in the adult *Drosophila* brain. *Curr. Biol.* **30**, 3167–3182.e4.
162. Saalfeld, S., Cardona, A., Hartenstein, V., and Tomančák, P. (2009). Catmaid: collaborative annotation toolkit for massive amounts of image data. *Bioinformatics* **25**, 1984–1986.
163. Sherer, L.M., Catudio Garrett, E., Morgan, H.R., Brewer, E.D., Sirrs, L.A., Shearin, H.K., Williams, J.L., McCabe, B.D., Stowers, R.S., and Cetrel, S.J. (2020). Octopamine neuron dependent aggression requires dVGLUT from dual-transmitting neurons. *PLoS Genet.* **16**, e1008609.
164. Crocker, A., Guan, X.J., Murphy, C.T., and Murthy, M. (2016). Cell-Type-Specific transcriptome analysis in the *drosophila* mushroom body reveals Memory-Related changes in gene expression. *Cell Rep.* **15**, 1580–1596.
165. Prokop, A., and Meinertzhagen, I.A. (2006). Development and structure of synaptic contacts in *Drosophila*. *Semin. Cell Dev. Biol.* **17**, 20–30.
166. Kubrak, O.I., Lushchak, O.V., Zandawala, M., and Nässel, D.R. (2016). Systemic corazonin signalling modulates stress responses and metabolism in *drosophila*. *Open Biol.* **6**, 160152.
167. Nichols, R., Schneuwly, S.A., and Dixon, J.E. (1988). Identification and characterization of a *drosophila* homologue to the vertebrate neuropeptide cholecystokinin. *J. Biol. Chem.* **263**, 12167–12170.
168. Söderberg, J.A.E., Carlsson, M.A., and Nässel, D.R. (2012). Insulin-Producing cells in the *drosophila* brain also express Satiety-Inducing Cholecystokinin-Like peptide, drosulfakinin. *Front. Endocrinol.* **3**, 109.
169. Cao, C., and Brown, M.R. (2001). Localization of an insulin-like peptide in brains of two flies. *Cell Tissue Res.* **304**, 317–321.
170. Nässel, D.R., and Vanden Broeck, J. (2016). Insulin/IGF signaling in *drosophila* and other insects: factors that regulate production, release and post-release action of the insulin-like peptides. *Cell. Mol. Life Sci.* **73**, 271–290.
171. Terhzaz, S., Rosay, P., Goodwin, S.F., and Veenstra, J.A. (2007). The neuropeptide SiFamide modulates sexual behavior in *drosophila*. *Biochem. Biophys. Res. Commun.* **352**, 305–310.
172. Kim, S., Wallace, M.L., El-Rifai, M., Knudsen, A.R., and Sabatini, B.L. (2022). Co-packaging of opposing neurotransmitters in individual synaptic vesicles in the central nervous system. *Neuron* **110**, 1371–1384.e7.
173. Johard, H.A.D., Enell, L.E., Gustafsson, E., Trifilieff, P., Veenstra, J.A., and Nässel, D.R. (2008). Intrinsic neurons of *drosophila* mushroom bodies express short neuropeptide f: relations to extrinsic neurons expressing different neurotransmitters. *J. Comp. Neurol.* **507**, 1479–1496.
174. Sukumar, S.K., Antonydhason, V., Molander, L., Sandakly, J., Umapathy, G., Mendoza-Garcia, P., Masudi, T., Schlosser, A., Nässel, D.R., Wegeiner, C., et al. (2023). The alk receptor tyrosine kinase regulates sparkly, a novel activity regulating neurosecretory protein in the *drosophila* CNS. Preprint at bioRxiv. <https://doi.org/10.1101/2023.06.02.543395>.
175. Kahsai, L., and Winther, A.M.E. (2011). Chemical neuroanatomy of the *drosophila* central complex: distribution of multiple neuropeptides in relation to neurotransmitters. *J. Comp. Neurol.* **519**, 290–315.
176. Hartenstein, V., Cruz, L., Lovick, J.K., and Guo, M. (2017). Developmental analysis of the dopamine-containing neurons of the *drosophila* brain. *J. Comp. Neurol.* **525**, 363–379.
177. Kahsai, L., Carlsson, M.A., Winther, A.M.E., and Nässel, D.R. (2012). Distribution of metabotropic receptors of serotonin, dopamine, GABA, glutamate, and short neuropeptide F in the central complex of *drosophila*. *Neuroscience* **208**, 11–26.
178. Takemura, S.-y., Xu, C.S., Lu, Z., Rivlin, P.K., Parag, T., Olbris, D.J., Plaza, S., Zhao, T., Katz, W.T., Umayam, L., et al. (2015). Synaptic circuits and their variations within different columns in the visual system of *drosophila*. *Proc. Natl. Acad. Sci. USA* **112**, 13711–13716.
179. Raghu, S.V., and Borst, A. (2011). Candidate glutamatergic neurons in the visual system of *drosophila*. *PLoS One* **6**, e19472.
180. Alekseyenko, O.V., Lee, C., and Kravitz, E.A. (2010). Targeted manipulation of serotonergic neurotransmission affects the escalation of aggression in adult male *drosophila melanogaster*. *PLoS One* **5**, e10806.
181. Cetrel, S.J., Leung, A., Lin, C.-Y., Perez, P., Chiang, A.-S., and Kravitz, E.A. (2010). Octopamine neuromodulatory effects on a social behavior decision-making network in *drosophila* males. *PLoS One* **5**, e13248.
182. Yang, J.S., Awasaki, T., Yu, H.-H., He, Y., Ding, P., Kao, J.-C., and Lee, T. (2013). Diverse neuronal lineages make stereotyped contributions to the *drosophila* locomotor control center, the central complex. *J. Comp. Neurol.* **521**, 2645–Spc1.

183. Lyu, C., Abbott, L.F., and Maimon, G. (2022). Building an allocentric travelling direction signal via vector computation. *Nature* **601**, 92–97.
184. Nässel, D.R. (2021). Leucokinin and associated neuropeptides regulate multiple aspects of physiology and behavior in drosophila. *Int. J. Mol. Sci.* **22**, 1940.
185. Troup, M., Yap, M.H., Rohrscheib, C., Grabowska, M.J., Ertekin, D., Randardiya, R., Kottler, B., Larkin, A., Munro, K., Shaw, P.J., and van Swinden, B. (2018). Acute control of the sleep switch in drosophila reveals a role for gap junctions in regulating behavioral responsiveness. *Elife* **7**, e37105.
186. Musso, P.-Y., Junca, P., and Gordon, M.D. (2021). A neural circuit linking two sugar sensors regulates satiety-dependent fructose drive in drosophila. *Sci. Adv.* **7**, eabj0186.
187. Hamid, A., Gattuso, H., Caglar, A.N., Pillai, M., Steele, T., Gonzalez, A., Nagel, K., and Syed, M.H. (2023). The RNA-binding protein, imp specifies olfactory navigation circuitry and behavior in drosophila. Preprint at bioRxiv. <https://doi.org/10.1101/2023.05.26.542522>.
188. De, J., Wu, M., Lambatan, V., Hua, Y., and Joiner, W.J. (2023). Re-examining the role of the dorsal fan-shaped body in promoting sleep in drosophila. *Curr. Biol.* **33**, 3660–3668.e4.
189. Huang, J., Zhang, W., Qiao, W., Hu, A., and Wang, Z. (2010). Functional connectivity and selective odor responses of excitatory local interneurons in drosophila antennal lobe. *Neuron* **67**, 1021–1033.
190. Yaksi, E., and Wilson, R.I. (2010). Electrical coupling between olfactory glomeruli. *Neuron* **67**, 1034–1047.
191. Berck, M.E., Khandelwal, A., Claus, L., Hernandez-Nunez, L., Si, G., Tabone, C.J., Li, F., Truman, J.W., Fetter, R.D., Louis, M., et al. (2016). The wiring diagram of a glomerular olfactory system. *Elife* **5**, e14859.
192. Chou, Y.-H., Yang, C.-J., Huang, H.-W., Liou, N.-F., Panganiban, M.R., Luginbuhl, D., Yin, Y., Taisz, I., Liang, L., Jefferis, G.S.X.E., and Luo, L. (2022). Mating-driven variability in olfactory local interneuron wiring. *Sci. Adv.* **8**, eabm7723.
193. Kumar, A., Bello, B., and Reichert, H. (2009). Lineage-specific cell death in postembryonic brain development of drosophila. *Development* **136**, 3433–3442.
194. Sen, S. (2019). Neurotransmitter identity: A question of lineage. *Elife* **8**, e47162.
195. Truman, J.W., Moats, W., Altman, J., Marin, E.C., and Williams, D.W. (2010). Role of notch signaling in establishing the hemilineages of secondary neurons in drosophila melanogaster. *Development* **137**, 53–61.
196. Jiang, Y., and Reichert, H. (2012). Programmed cell death in type II neuroblast lineages is required for central complex development in the drosophila brain. *Neural Dev.* **7**, 3.
197. Marin, E.C., Watts, R.J., Tanaka, N.K., Ito, K., and Luo, L. (2005). Developmentally programmed remodeling of the *Drosophila* olfactory circuit. *Development* **132**, 725–737.
198. Sullivan, L.F., Warren, T.L., and Doe, C.Q. (2019). Temporal identity establishes columnar neuron morphology, connectivity, and function in a drosophila navigation circuit. *Elife* **8**, e43482.
199. Lovick, J.K., Ngo, K.T., Omoto, J.J., Wong, D.C., Nguyen, J.D., and Hartenstein, V. (2013). Postembryonic lineages of the *Drosophila* brain: I. development of the lineage-associated fiber tracts. *Dev. Biol.* **384**, 228–257.
200. Wong, D.C., Lovick, J.K., Ngo, K.T., Borisuthirattana, W., Omoto, J.J., and Hartenstein, V. (2013). Postembryonic lineages of the *Drosophila* brain: II. identification of lineage projection patterns based on MARCM clones. *Dev. Biol.* **384**, 258–289.
201. Yu, H.-H., Awasaki, T., Schroeder, M.D., Long, F., Yang, J.S., He, Y., Ding, P., Kao, J.-C., Wu, G.Y.-Y., Peng, H., et al. (2013). Clonal development and organization of the adult *Drosophila* central brain. *Curr. Biol.* **23**, 633–643.
202. Kandimalla, P., Omoto, J.J., Hong, E.J., and Hartenstein, V. (2023). Lineages to circuits: the developmental and evolutionary architecture of information channels into the central complex. *J. Comp. Physiol. A Neuroethol. Sens. Neural Behav. Physiol.* **209**, 679–720.
203. Cardona, A., Saalfeld, S., Schindelin, J., Arganda-Carreras, I., Preibisch, S., Longair, M., Tomancak, P., Hartenstein, V., and Douglas, R.J. (2012). TrakEM2 software for neural circuit reconstruction. *PLoS One* **7**, e38011.
204. Rohlfing, T., and Maurer, C.R., Jr. (2003). Nonrigid image registration in shared-memory multiprocessor environments with application to brains, breasts, and bees. *IEEE Trans. Inf. Technol. Biomed.* **7**, 16–25.
205. Bello, B.C., Izergina, N., Caussinus, E., and Reichert, H. (2008). Amplification of neural stem cell proliferation by intermediate progenitor cells in drosophila brain development. *Neural Dev.* **3**, 5.
206. Boone, J.Q., and Doe, C.Q. (2008). Identification of drosophila type II neuroblast lineages containing transit amplifying ganglion mother cells. *Dev. Neurobiol.* **68**, 1185–1195.
207. Bowman, S.K., Rolland, V., Betschinger, J., Kinsey, K.A., Emery, G., and Knoblich, J.A. (2008). The tumor suppressors brat and numb regulate transit-amplifying neuroblast lineages in drosophila. *Dev. Cell* **14**, 535–546.
208. Baker, C.A., McKellar, C., Pang, R., Nern, A., Dorkenwald, S., Pacheco, D.A., Eckstein, N., Funke, J., Dickson, B.J., and Murthy, M. (2022). Neural network organization for courtship-song feature detection in drosophila. *Curr. Biol.* **32**, 3317–3333.e7.
209. Eichler, K., Hampel, S., Alejandro-García, A., Calle-Schuler, S.A., Santana-Cruz, A., Kmecova, L., Blagburn, J.M., Hooper, E.D., and Seeds, A.M. (2023). Somatotopic organization among parallel sensory pathways that promote a grooming sequence in drosophila. Preprint at bioRxiv. <https://doi.org/10.1101/2023.02.11.528119>.
210. Engert, S., Sterne, G.R., Bock, D.D., and Scott, K. (2022). Drosophila gustatory projections are segregated by taste modality and connectivity. *Elife* **11**, e78110.
211. Li, F., Lindsey, J.W., Marin, E.C., Otto, N., Dreher, M., Dempsey, G., Stark, I., Bates, A.S., Pleijzier, M.W., Schlegel, P., et al. (2020a). The connectome of the adult drosophila mushroom body provides insights into function. *Elife* **9**, e62576.
212. Chiang, A.-S., Lin, C.-Y., Chuang, C.-C., Chang, H.-M., Hsieh, C.-H., Yeh, C.-W., Shih, C.-T., Wu, J.-J., Wang, G.-T., Chen, Y.-C., et al. (2011). Three-dimensional reconstruction of brain-wide wiring networks in drosophila at single-cell resolution. *Curr. Biol.* **21**, 1–11.